Journal of the Meteorological Society of Japan

EARLY ONLINE RELEASE

This is a PDF of a manuscript that has been peer-reviewed and accepted for publication. As the article has not yet been formatted, copy edited or proofread, the final published version may be different from the early online release.

This pre-publication manuscript may be downloaded, distributed and used under the provisions of the Creative Commons Attribution 4.0 International (CC BY 4.0) license. It may be cited using the DOI below.

The DOI for this manuscript is
DOI:10.2151/jmsj.2025-013
J-STAGE Advance published date: January 15, 2025
The final manuscript after publication will replace the preliminary version at the above DOI once it is available.

Seasonality in the ENSO-independent influence of tropical Indian Ocean sea surface temperature anomalies on western North Pacific tropical cyclone genesis

Jinjie SONG[1]

Nanjing Joint Institute for Atmospheric Sciences, Chinese Academy of Meteorological Sciences, Nanjing, China
State Key Laboratory of Severe Weather, Chinese Academy of Meteorological Sciences, Beijing, China

Philip J. KLOTZBACH

Department of Atmospheric Science, Colorado State University, Fort Collins, CO, USA

Yi–Fan WANG

Nanjing Joint Institute for Atmospheric Sciences, Chinese Academy of Meteorological Sciences, Nanjing, China
State Key Laboratory of Severe Weather, Chinese Academy of Meteorological Sciences, Beijing, China

and

Yihong DUAN

State Key Laboratory of Severe Weather, Chinese Academy of Meteorological Sciences, Beijing, China

December 30, 2024

----

1) Corresponding author: Jinjie Song, Editorial Office, Nanjing Joint Institute for Atmospheric Sciences, 8 Yushun Road, Nanjing, China, 210041
Email: songjinjie@qq.com

Abstract

This study investigates the seasonality in the influence of tropical Indian Ocean (IO) sea surface temperature (SST) anomalies independent of El Niño-Southern Oscillation (ENSO) on tropical cyclone (TC) genesis over the western North Pacific (WNP) from 1979–2022. We focus on the dominant pattern of Indian Ocean SST variability – the Indian Ocean basin mode (IOBM) independent of ENSO. We separate the WNP TC-active period into the early season April–June (AMJ), the peak season July–September (JAS) and the late season October–December (OND). When the preceding and simultaneous influence of ENSO is removed, the correlation between WNP TC frequency and the ENSO-independent IOBM has considerable seasonality, with a significant correlation during JAS but an insignificant correlation during AMJ and OND. In warm ENSO-independent IOBM phases, WNP TC genesis is significantly suppressed over the region of 15°–25°N and 140°–155°E during JAS, while there are insignificant changes in WNP TC genesis during AMJ and OND.

In a warm IOBM independent of ENSO, significant TC genesis reductions during JAS are primarily driven by significantly decreased 850-hPa relative vorticity and significantly increased 500-hPa vertical velocity (e.g., downward motion), while insignificant TC genesis changes during AMJ and OND are consistent with weak environmental changes over the WNP. These features can be linked to the seasonality in Indo-Pacific large-scale circulation anomalies induced by the ENSO-independent IOBM. In analogy to the mechanism of the Indo-western Pacific ocean capacitor mode, warm IO SSTAs independent of ENSO can lead to an anomalous low-level

anticyclone over the WNP during both AMJ and JAS, with their remote influence dissipating during OND. The ENSO-independent warm IO-driven anomalous WNP anticyclone is weak and insignificant during AMJ but is strong and significant during JAS, likely due to a smaller amplitude of IOBM-induced SSTAs independent of ENSO during AMJ than during JAS.

Keywords: tropical cyclone, western North Pacific, tropical Indian Ocean

1. Introduction

Tropical cyclones (TCs) are one of the most severe natural disasters, often associated with strong winds, heavy rainfall, and storm surge that can cause significant societal and economic damage in coastal and adjacent inland regions. The western North Pacific (WNP) is the most TC-active basin worldwide, where approximately one-third of global TCs form on an annually-averaged basis (Lee et al., 2012). Given increased concern about the impact of climate change, additional focus has been paid to WNP TC activity changes on interannual timescales (Walsh et al., 2016).

El Niño-Southern Oscillation (ENSO) has been considered to be the primary mode influencing interannual changes in WNP TC genesis (Emanuel, 2018). There are two major ENSO flavors: eastern Pacific (EP) ENSO and central Pacific (CP) ENSO, with peak anomalous sea surface warming/cooling centered over the eastern equatorial Pacific and the central equatorial Pacific, respectively (e.g., Timmermann et al., 2018). In general, EP El Niño (EP La Niña) leads to a significant southeastward (northwestward) shift in average WNP TC genesis location (e.g., Lander, 1994; Chan, 1985, 2000; Saunders et al., 2000; Wang and Chan, 2002; Li and Zhou, 2012), while CP El Niño (CP La Niña) results in an almost basinwide enhancement (suppression) of WNP TC genesis (e.g., Chen and Tam, 2010; Kim et al., 2011; Wang et al., 2013; Li and Wang, 2014; Zhang et al., 2015; Patricola et al., 2018). These ENSO-induced changes in TC genesis can be explained by different large-scale anomalous low-level circulations over the WNP, with a Gill response to the maximum oceanic warming/cooling occurring over the eastern or central equatorial Pacific (Gill, 1980).

The Pacific meridional mode (PMM) is another climate mode over the tropical Pacific that influences WNP TC genesis (e.g., Zhang et al., 2016; Gao et al., 2018; Gao et al., 2020; Zhang et al., 2020; Wu et al., 2020; Fu et al., 2023). During positive (negative) phases of the PMM, TC genesis is generally enhanced (suppressed) over almost the entire WNP, mainly because of an anomalous basinwide low-level cyclonic (anticyclonic) circulation. Given the strong relationship between the PMM and CP ENSO (Stuecker, 2018), there is still debate on the significance of the PMM-TC relationship independent of ENSO (e.g., Qian et al., 2019; Takaya et al., 2019; Zhang et al., 2020; Wu et al., 2020).

There are also remote regions that have been shown to modulate interannual changes in WNP TC genesis. Among these are sea surface temperature (SST) anomalies (SSTAs) over the Indian Ocean (IO) (e.g., Du et al., 2011; Zhan et al., 2011a; Zhan et al., 2011b; Tao et al., 2012; Kosaka et al., 2013; Zhan et al., 2014; Ha et al., 2015; Zheng et al., 2016; Takaya et al., 2018; Ueda et al., 2018; Huangfu et al., 2018; Zhao et al., 2019; Huangfu et al., 2019). Several of these studies examined TC genesis anomalies in positive and negative IO SSTA years without excluding concurrent ENSO events (Zhan et al., 2011a; Zhan et al., 2011b; Tao et al., 2012; Zheng et al., 2016). Given the strong relationship between ENSO and IO SSTAs (e.g., Yang et al., 2007; Xie et al., 2009), other studies have either investigated the sole influence of IO SSTAs on TC genesis after removing the simultaneous ENSO effect (Zhan et al., 2014; Ha et al., 2015; Huangfu et al., 2018) or have focused on the relationship between IO SSTAs and TC activity in ENSO-decaying years (Du et al., 2011; Kosaka et al., 2013; Takaya et al., 2018; Ueda et al., 2018; Zhao et al., 2019; Huangfu et al., 2019). Regardless of analysis method, the consensus is that IO warming (cooling) can induce a basinwide suppression (enhancement) of TC genesis over the WNP. The Indo-western Pacific Ocean capacitor mechanism (IPOC; e.g., Xie et al., 2009; Xie et al., 2016) is often used to link SSTAs over the IO and environmental changes over the WNP. Tropical IO warming excites a warm equatorial Kelvin wave that moves eastward into the equatorial western Pacific. This wave induces surface convergence on the equator and surface divergence off the equator, triggering a large-scale anomalous low-level anticyclone over the WNP. This anticyclone and its associated descending motion can suppress WNP TC activity.

Recently, several studies have noted the seasonality of WNP TC genesis changes, modulated by different ENSO flavors. Wang et al. (2013) reported that EP ENSO contributed to an obvious southeast-northwest dipole pattern of WNP TC genesis anomalies only during July–September (JAS). Significant EP ENSO-induced TC genesis changes mainly occurred over the southern WNP during April–June (AMJ) and over the western WNP during October–December (OND). There were no significant CP ENSO-induced TC genesis changes over most of the WNP during AMJ, while CP ENSO strongly influenced WNP TC genesis during JAS and OND. By comparison, Choi et al. (2019) showed that EP El Niño caused a southward (southeastward) migration of WNP TC genesis during boreal summer (autumn). CP El Niño resulted in a basinwide enhancement of WNP TC genesis during boreal summer, while it led to significant increases (decreases) in TC genesis over the western (eastern) WNP during boreal autumn. Furthermore, Wang et al. (2013) and Choi et al. (2019) both concluded that the seasonality in the relationship between ENSO and WNP TC genesis was primarily a result of seasonal changes in the ENSO background state.

Fu et al. (2023) found that the relationship between the PMM and WNP TC genesis was seasonally-dependent, due to different responses of WNP environmental conditions to PMM-related SST changes and different climatological locations for the TC main development region (MDR). During January–July, positive PMM-related SST warming in the subtropical North Pacific predominantly induced TC-favoring (TC-suppressing) conditions over the eastern (western) WNP. There was a significant PMM-TC frequency correlation during January–April, given that the TC MDR is limited over the eastern WNP. By contrast, there was only a weak PMM-TC frequency correlation during May–July, because the TC MDR during those months spanned the entire tropical WNP. During August–December, positive PMM-related SST cooling over the equatorial eastern Pacific resulted in a basinwide WNP TC-favorable environment, leading to a significant PMM-TC frequency correlation.

Like the PMM, the dominant mode of IO SST variability often develops in boreal winter, peaks in the following spring, and persists into summer (e.g., Klein et al., 1999; Alexander et al., 2002; Li et al., 2003; Yang et al., 2007; Xie et al., 2016). This annual cycle suggests that the influence of IO SSTAs on WNP TC genesis may vary with season. Some studies (e.g., Du et al., 2011; Zhan et al., 2011a; Zhan et al., 2011b; Tao et al., 2012; Zhan et al., 2014; Ha et al., 2015; Zheng et al., 2016; Huangfu et al., 2018; Huangfu et al., 2019) have considered IO SSTAs as a seasonally-consistent forcing, with most attention focusing on the effect of IO SSTAs on WNP TC genesis during the peak TC season or the full TC season. By comparison, other studies (Kosaka et al., 2013; Takaya et al., 2018; Ueda et al., 2018; Zhao et al., 2019) have noticed the seasonality in the relationship between IO SSTAs and WNP TC frequency, with a significant (insignificant) warm IO-induced suppression of TC activity before (after) the early boreal winter. Ueda et al. (2018) further linked this seasonality to the weakening of an anomalous anticyclone over the western Pacific that was anchored with positive SSTAs over the IO after September.

Given that all these studies focused on ENSO decaying years, the seasonality in the relationship between IO SSTAs and WNP TC activity is likely to be influenced by the evolutionary characteristics of ENSO. However, IO SSTAs can modulate the WNP environment without the occurrence of ENSO. By performing a numerical experiment without ENSO-related influences, Kosaka et al. (2013) found an internal atmosphere-ocean coupled IPOC mode in the Indo-Pacific region. Some recent studies (e.g., Takaya et al., 2020; Zhou et al., 2021; Du et al., 2022) also suggested that the Indian Ocean dipole (IOD) could cause the IPOC mode without a strong ENSO event. As noted in these studies, the IPOC could work without ENSO forcing, including the coupling of the IO warming and the WNP anomalous anticyclone. This so-called ENSO-independent IPOC that is driven by other factors (e.g., the IOD) may be similar to the ENSO-dependent IPOC. It is likely that when excluding ENSO's influence, the seasonality in the relationship between IO SSTAs and WNP TC activity is driven by seasonal changes in the IPOC. Therefore, this study extends prior research by excluding the potential influence of ENSO and then examining the differing responses of WNP TC genesis to IO SSTAs during different seasons. We also investigate the corresponding physical mechanisms, particularly IPOC changes in different seasons. We focus on the dominant mode of IO SST changes, which has been termed the Indian Ocean basin mode (IOBM; e.g., Klein et al., 1999; Yang et al., 2007).

The remainder of this study is organized as follows. Section 2 describes the data and methodology. Sections 3 and 4 discuss the seasonality of IOBM-induced changes for WNP TC genesis and for environmental conditions, respectively. Section 5 summarizes and concludes.

2. Data and methodology

2.1 Data

a. TC data

WNP TC best track data from 1979–2022 are obtained from the International Best Track Archive for Climate Stewardship (IBTrACS) v4 dataset (Knapp et al., 2010). TC data prior to 1979 are not used, due to lower reliability of TC observations due to lack of global satellite coverage (Kossin et al., 2014). To further minimize the uncertainty in TC data, this study only considers TC cases simultaneously recorded by all four warning agencies operationally providing TC best tracks over the full WNP, including the Joint Typhoon Warning Center, the Japan Meteorological Agency, the China Meteorological Administration, and the Hong Kong Observatory. TC cases that are not recorded by all four agencies are excluded. Only TCs with a lifetime maximum intensity (LMI) of at least tropical storm intensity (≥34 kt) are recorded in the TC best track from the Japan Meteorological Agency, while the other three agencies record different numbers of TCs with an LMI <34 kt. Therefore, tropical storms (34 kt≤LMI<64 kt) and typhoons (LMI≥64 kt) are considered in this study, while all tropical depressions (LMI< 34kt) are excluded. TC genesis is identified as the first record that is simultaneously reported by all four agencies, as suggested by Song and Klotzbach (2018). Gridded TC genesis frequencies (TCGFs) are first obtained by counting TC genesis numbers over a 5°×5° grid and are then spatially smoothed through the method proposed by Kim et al. (2011).

b. Oceanic and atmospheric data

Monthly mean SST data over a 1°×1° grid are calculated from the Hadley Centre Sea Ice and Sea Surface Temperature dataset (HadISST; Rayner et al., 2003). SSTAs are defined by subtracting the corresponding long-term SST trends from 1979 to 2022 to remove any global warming signal. Monthly mean atmospheric conditions are derived from the fifth generation European Centre for Medium-Range Weather Forecasts (ECMWF) reanalysis of the global climate (ERA5; Hersbach et al., 2020), with a horizontal resolution of 0.25°×0.25°.

2.2 TC genesis potential index

We use the dynamic genesis potential index (DGPI) developed by Wang and

Murakami (2020) to measure the joint influence of large-scale environmental conditions on TC genesis. The DGPI has shown greater skill in capturing interannual variability of WNP TC genesis than the genesis potential index proposed by Emanuel and Nolan (2004) (Wang and Murakami, 2020). The DGPI consists of four atmospheric variables: 850–200-hPa vertical wind shear (VWS), 850-hPa absolute vorticity, 500-hPa vertical velocity and the 500-hPa meridional gradient of zonal wind (MGZW). All these variables are calculated from ERA5. Greater DGPIs commonly correspond to more TC geneses, resulting from positive anomalies of absolute vorticity and negative anomalies of VWS, vertical velocity and MGZW.

2.3 IOBM indices

a. Definition

The original IOBM index is calculated as the average SSTA over the tropical IO (20°S–20°N, 40°–100°E) (e.g., Xie et al., 2009). The ENSO index is computed as the SSTA averaged over the Niño-3.4 region (5°S–5°N, 170°–120°W). As shown in Figure 1a, there is a significant positive simultaneous correlation between the monthly IOBM and ENSO indices from 1979–2022 (r=0.56; p<0.01). Moreover, the correlation between monthly ENSO and IOBM indices reaches its maximum at the time when the IOBM lags ENSO by approximately three months, as documented in previous publications (e.g., Yang et al., 2007; Xie et al., 2009). This also corresponds to ENSO often maturing in boreal winter and the IOBM peaking in boreal spring. The regression-based method proposed by An (2003) has been widely used to linearly remove the signal of one index from another index. Here, we utilize three formulas to exclude ENSO's effect on the IOBM index:

$$I_{\mathrm{IOBM}}^{1} = I_{\mathrm{IOBM}}^{o} - I_{\mathrm{ENSO}}^{0} \times \mathrm{cov}\left(I_{\mathrm{IOBM}}^{o}, I_{\mathrm{ENSO}}^{0}\right) / \mathrm{var}\left(I_{\mathrm{ENSO}}^{0}\right), \quad (1)$$

$$I_{\mathrm{IOBM}}^{2} = I_{\mathrm{IOBM}}^{o} - I_{\mathrm{ENSO}}^{\mathrm{NDJ}} \times \mathrm{cov}\left(I_{\mathrm{IOBM}}^{o}, I_{\mathrm{ENSO}}^{\mathrm{NDJ}}\right) / \mathrm{var}\left(I_{\mathrm{ENSO}}^{\mathrm{NDJ}}\right), \quad (2)$$

$$I_{\mathrm{IOBM}}^{3} = I_{\mathrm{IOBM}}^{2} - I_{\mathrm{ENSO}}^{0} \times \mathrm{cov}\left(I_{\mathrm{IOBM}}^{2}, I_{\mathrm{ENSO}}^{0}\right) / \mathrm{var}\left(I_{\mathrm{ENSO}}^{0}\right), \quad (3)$$

where cov(·) and var(·) denote covariance and variance, respectively. I_{ENSO}^{0} and $I_{\mathrm{ENSO}}^{\mathrm{NDJ}}$ are the simultaneous and preceding November–January (NDJ) ENSO indices, respectively. I_{IOBM}^{o} is the original IOBM index, while I_{IOBM}^{1} (I_{IOBM}^{2}) denotes the IOBM index when the influence of the simultaneous (preceding NDJ) ENSO is linearly removed in I_{IOBM}^{o}. Furthermore, I_{IOBM}^{3} represents the IOBM index when excluding the influence of the simultaneous ENSO on I_{IOBM}^{2}, which minimizes both the simultaneous and preceding effect of ENSO.

b. Comparison

Figure 1b–d highlights that during any individual season (AMJ, JAS or OND), there is a significant relationship between the original IOBM and ENSO indices. During AMJ and JAS, the preceding ENSO plays a greater role in influencing the IOBM than the simultaneous ENSO (Figure 1b, c). During OND, the IOBM-ENSO relationship becomes more simultaneous, with a simultaneous correlation that is much larger than during AMJ and JAS (Figure 1d). In particular, there is only a weak and insignificant correlation between the preceding winter ENSO index and the OND IOBM index.

The above results mean that the original IOBM indices during different seasons are primarily controlled by ENSO at different lead times. As a result, when simultaneous ENSO's influence is removed, there remains a significant correlation of the IOBM during AMJ and JAS with the preceding ENSO (Figure 1b, c). When the influence of the preceding NDJ ENSO is removed, the simultaneous IOBM-ENSO correlation is still large during OND and even becomes significant during JAS (Figure 1c, d). These results imply that Eqns. (1) and (2) can only partially exclude ENSO's effect on the IOBM. By comparison, after applying Eqn. (3), the IOBM during any one season of AMJ, JAS and OND only weakly correlate with both the preceding ENSO and the simultaneous ENSO (Figure 1b–d). Additionally, the correlation between the monthly IOBM and ENSO indices during 1979–2022 becomes weak and insignificant, when ENSO leads the IOBM (Figure 1a). Consequently, Eqn. (3) can effectively remove both the simultaneous and preceding influences of ENSO on the IOBM. Therefore, the IOBM index obtained by Eqn. (3) is considered as ENSO-independent in the following sections.

c. Classification

Takaya et al. (2021) showed that a warm IO could occur concurrently with either El Niño or La Niña. We thus identify positive, neutral and negative IOBM seasons during 1979–2022 by using the following two procedures. First, the seasons with 3-month averaged Niño-3.4 SSTAs > +0.5°C or < -0.5°C are excluded. Second, a threshold of 0.6 standard deviations, which roughly corresponds to a 0.5°C change of the Niño-3.4 SSTA, is applied to the ENSO-independent IOBM index (approximately 0.3ºC change in this index) to separate the remaining seasons into positive, neutral and negative IOBM phases. Tables 1–3 list the identified AMJ, JAS and OND seasons with positive, neutral and negative IOBM phases.

2.4 Significance test

Statistical significance of correlation coefficients, regression coefficients and the differences in means between two samples is estimated by using a two-tailed Student's *t*-test. In evaluating significance of correlation coefficients, the effective sample size proposed by Bretherton et al. (1999) is applied to account for autocorrelation of the individual time series.

3. Seasonality of IOBM-induced changes in TC genesis

Figure 2a shows a significant inverse relationship between the annual WNP TC number and the annual mean IOBM index during 1979–2022, regardless of which IOBM index is considered. This is consistent with previous publications which found a suppression of WNP TC genesis in warm IO years (e.g., Tao et al., 2012) or in TC-active seasons with warm IO SSTAs (e.g., Du et al., 2011; Zhan et al., 2011a; Zhan et al., 2011b; Tao et al., 2012; Zhan et al., 2014; Ha et al., 2015; Zheng et al., 2016). However, the IOBM-TC relationship exhibits obvious seasonality. The correlation between TC number and the original IOBM index is significant from mid spring to early autumn but insignificant for the remainder of the year (Figure 2b). The most significant correlation occurs during AMJ (r=-0.50; p<0.01).

By comparison, the IOBM-TC relationship changes when ENSO's impact is excluded. When removing the influence of the simultaneous ENSO, the IOBM-TC correlation becomes insignificant during spring, while changing less during other seasons. When removing the influence of the preceding NDJ ENSO, the IOBM-TC correlation becomes insignificant during mid spring to summer but remains significant during early autumn. When considering the correlation of TC number with the ENSO-independent IOBM index, which removes both the influences of the simultaneous and preceding NDJ ENSO on the IOBM, the IOBM-TC relationship becomes weak and insignificant from mid spring to early summer, while remaining significant from mid summer to early autumn. This underscores the significant IO-mediated influence of ENSO, as noted by previous studies. Note that the seasonal change in the correlation of TC number with the ENSO-independent IOBM index is more similar to that with the IOBM index excluding the influence of the preceding NDJ ENSO during spring–summer, while it is more like that with the IOBM index excluding the influence of the simultaneous ENSO during autumn. This means that ENSO modulates the IOBM-TC relationship mainly through its delayed effect during spring and summer but through its simultaneous effect during autumn. Additionally, seasonal distributions of the IOBM-TC relationship as shown in Figure 2b differ from the PMM-TC relationship found in Fu et al. (2023), where an insignificant correlation was reported during May–July. The difference in the seasonality of these relationships implies that interannual variability in WNP TC number during different seasons is likely controlled by different climate modes.

Following Wang et al. (2013), we now examine three TC seasons: the early season (AMJ), the peak season (JAS) and the late season (OND). During AMJ, the climatological TC MDR displays a northwest-southeast orientation, with a majority of

TCs occurring south of 20°N (Figure 3a). When the original IOBM index is considered, there is a basinwide suppression of WNP TC genesis in a warm IOBM, with significant TCGF decreases west of 150°E (Figure 4a), This pattern resembles warm IOBM-induced TCGF changes, if simultaneous ENSO's influence is removed (Figure 4b). By comparison, when removing the influence of the preceding NDJ ENSO, warm IOBM-induced TCGF reductions weaken and become insignificant over most of the WNP (Figure 4c). Similarly, TCGF decreases induced by warm ENSO-independent IOBM are concentrated over the region of 5°–25°N and 110°–170°E, but are weak and insignificant (Figure 4d). Consequently, there is a weak and insignificant correlation between TC number and the ENSO-independent IOBM index (r=-0.13; p=0.39). These results mean that the suppressing influence of the IOBM on WNP TC genesis during AMJ predominately occurs due to the delayed effect of ENSO, with the ENSO-independent IOBM itself playing only a minor role.

During JAS, the climatological TC MDR shifts northward and spans the latitudinal belt of 10°–25°N (Figure 3b). Consistent with Tao et al. (2012), a warm IOBM is associated with strong TCGF decreases over the subtropical WNP (10°–30°N, 120°–170°E) and weak TCGF changes over other parts of the WNP, regardless of which IOBM index is considered (Figure 5). As a result, basinwide TC frequency during JAS is significantly anti-correlated with the ENSO-independent IOBM index (r=-0.31; p=0.04). These results imply that neither the preceding ENSO nor the simultaneous ENSO has a significant impact on the IOBM-TC relationship during JAS.

During OND, the climatological TC MDR retreats southward (Figure 3c). When using the original IOBM index, there are TCGF increases east of 150°E and TCGF decreases west of 150°E (Figure 6a). This structure is similar to the east-west dipolar pattern in TCGF changes induced by El Niño, likely due to the strong simultaneous IOBM-ENSO correlation as shown in Figure 1d. This feature remains almost unchanged when the influence of the preceding NDJ ENSO on the IOBM is excluded (Figure 6c). However, when removing the influence of the simultaneous ENSO, a warm IOBM is associated with TCGF increases west of 140°E and decreases east of 140°E (Figure 6b). This pattern is also shown for the ENSO-independent IOBM-induced TCGF changes, with TCGF increases over the region of 5°–25°N and 105°–140°E and TCGF decreases over the region of 5°–30°N and 140°–160°E (Figure 6d). Given these insignificant TCGF changes, there is an insignificant correlation between WNP TC number and the ENSO-independent IOBM index during OND (r=-0.03; p=0.83). These results mean that in contrast to AMJ, ENSO influences the IOBM-TC relationship during OND mainly through its simultaneous effect. The IOBM-induced TCGF changes exhibit almost opposite structures before and after removing the simultaneous effect of ENSO on the IOBM.

We focus on the results related to the ENSO-independent IOBM index in the subsequent analyses, given that several studies have already analyzed the IOBM-TC relationship when ENSO's impact is not excluded (e.g., Du et al., 2011; Kosaka et al., 2013; Takaya et al., 2018; Ueda et al., 2018; Zhao et al., 2019; Huangfu et al., 2019). Tables 1–3 list basinwide WNP TC frequencies during the identified positive, neutral and negative IOBM seasons during 1979–2022. During AMJ, compared with neutral phase, there are -0.9 (p=0.19) TCs in positive IOBM and +1.1 (p=0.21) TCs in negative IOBM, while the TC frequency difference between positive and negative IOBM phases is -2.0 (p=0.37). The corresponding values are -3.7 (p<0.01), 4.3 (p<0.01) and -8.0 (p<0.01) during JAS and 0.5 (p=0.62), 0.2 (p=0.88) and 0.3 (p=0.86) during OND. Consistent with the IOBM-TC correlations shown in Figure 2b, TC frequency differences between positive and negative IOBM phases are significant during JAS but insignificant during AMJ and OND.

Figure 7 displays WNP TCGF differences between positive, neutral and negative phases of the IOBM. In general, regardless of the season considered, TCGF differences for positive IOBM versus neutral phases and for positive and negative IOBM phases exhibit a similar pattern to regressions of TCGFs onto the IOBM index, while those for negative IOBM versus neutral phases show a nearly mirror image. Significant TCGF differences only appear during JAS, mainly over the region of 15°–25°N, 140°–155°E (Figure 7d–f). Hong et al. (2010) has reported that the amplitude of the basinwide IO warming is on average greater than that of the cooling. However, this asymmetry occurs only when ENSO is concurrent with the IOD, while it becomes negligible during the ENSO-only and the IOD-only events. Cai and van Rensch (2013) has found that the asymmetry in the IOBM modulation effect is primarily a result of the asymmetry in ENSO's influence. Consistent with these findings, the IOBM's influence on WNP TC genesis is nearly symmetric, with almost opposite TCGF changes in positive and negative IOBM phases when excluding the ENSO signal in our IOBM index. Given relatively few samples in some of our IOBM groups (Tables 1–3), we focus on regressions of environmental factors in the following sections.

4. Seasonality of IOBM-induced changes in environmental conditions

Figure 8 displays climatological mean DGPIs and the regressions of DGPIs onto the IOBM index during different seasons. As noted in previous studies (e.g., Wang et al., 2013; Choi et al., 2019; Fu et al., 2023), DGPIs can well capture the seasonal migration of the climatological TC MDR over the WNP (Figure 8a, c, e). In general, the regressed DGPIs (Figure 8b, d, f) exhibit a similar distribution to the regressed TCGFs during each season (Figure 4d, Figure 5d, and Figure 6d). For a warm IOBM, weak TCGF and DGPI decreases during AMJ are both concentrated from 10° to 20°N and east of 150°E (Figure 8b). There are significant decreases in DGPI during JAS over the region of 15°–30°N, 125°–155°E, an area slightly larger than the region with significantly decreased TCGF (Figure 8d). There are insignificant DGPI increases west of 140°E and insignificant DGPI decreases west of 140°E during OND, similar to the observed TCGF changes (Figure 8f). As shown in Table 4, regional TCGF changes are significantly correlated with regional mean DGPIs during each season. These results imply that the seasonality of the ENSO-independent influence of the IOBM on WNP TC genesis can be largely explained by the IOBM-induced seasonal changes in environmental conditions.

Figures 9–11 show regressions of environmental variables constituting the DGPI during AMJ, JAS and OND, respectively. During AMJ, there are no significant changes in 850–200-hPa VWS, 500-hPa vertical velocity and 850-hPa relative vorticity over most of the WNP (Figure 9a, c, d), while significant changes in 500-hPa MGZW mainly occur at higher latitudes (Figure 9b). This means that the IOBM has a small impact on environmental conditions over the tropical WNP, when the influence of the preceding ENSO is excluded. This also underlines that ENSO-induced IOBM warming predominates in controlling WNP TC activity in AMJ. There are weak increases in vertical velocity (e.g., sinking motion) and weak decreases in vorticity south of 25°N and west of 155°E, corresponding to insignificant decreases in TCGF and DGPI (Figure 9c, d). By comparison, weak decreases in MGZW are found over this region (Figure 9b), which enhances TC genesis according to the DGPI. These results imply that the TC-suppressing effects of vertical velocity and vorticity surpass the TC-favoring effect of MGZW during AMJ.

In general, changes in WNP environmental variables are more significant during JAS than during AMJ (Figure 10). During JAS, although significant increases and decreases in VWS are concentrated over the eastern and western parts of the WNP, respectively, they appear near the boundary of the region with significant TCGF reductions (15°–25°N and 140°–155°E) (Figure 10a). Over this region, most of the MGWZ increases are insignificant (Figure 10b), while there are significant increases in vertical velocity (e.g., sinking motion) and significant decreases in vorticity (Figure 10c, d). These results imply that the IOBM modulates WNP TC genesis during JAS primarily by modulating vertical velocity and vorticity.

During OND, the changes in the four factors comprising the WNP DGPI are generally insignificant (Figure 11). There are weak changes in VWS and MGZW south of 20°N and west of 155°E (Figure 11a, b), where TCs form more frequently during OND (Figure 3c). Although significant decreases in vertical velocity (e.g., upward motion) are shown over a small domain of 20°–30°N and 140°–145°E, they are located outside the TC main development region (Figure 11c). Moreover, despite weak and insignificant changes, TCGF increases west of 140°E correspond to vertical velocity decreases and vorticity increases, while TCGF decreases east of 140°E correspond to vertical velocity increases and vorticity decreases (Figure 11c, d). These results indicate that similar to the IOBM's impact during AMJ, the IOBM does not significantly modulate the WNP environment during OND.

We now focus on regions with larger ENSO-independent IOBM-induced TCGF changes during different seasons. Table 4 gives correlation coefficients between regional TC frequency and regional mean environmental factors. During AMJ, TC frequency over the region of 5°–25°N and 110°–170°E is significantly correlated with all four factors comprising the DGPI. During JAS, TC frequency over the region of 10°–30°N and 120°–170°E is significantly correlated with MGWZ, vertical velocity and relative vorticity. During OND, TC frequency over the region of 5°–25°N and 105°–140°E is significantly correlated with MGWZ, vertical velocity and relative vorticity, while TC frequency over the region of 5°–30°N and 140°–160°E is significantly correlated with vertical velocity and relative vorticity. In all cases, vertical velocity and relative vorticity correlate most significantly with TC frequency.

Based on the above analyses, we can conclude that changes in 500-hPa vertical velocity and 850-hPa relative vorticity play a dominant role in the modulation of WNP TC genesis by the IOBM, regardless of the season considered.

Changes in these two variables can be further linked to IOBM-induced environmental changes over the Indo-Pacific region. During any of the three seasons investigated (AMJ, JAS or OND), positive SSTAs over the IO can locally trigger anomalously deep atmospheric convection, associated with eastward-propagating Kelvin waves (Figure 12). However, there is a notable remote influence of the IOBM only during JAS, while the IOBM's influence is limited over the IO during AMJ and OND. During AMJ and JAS, Kelvin wave-related anomalous low-level easterlies oppose climatological low-level westerlies (Figure 13a, b), suppressing surface evaporation and further enhancing IO warming through a wind-evaporation-SST (WES) feedback (Xie and Philander, 1994) (Figure 12a, c). This positive feedback favors both warm SSTs and Kelvin waves propagating into the western Pacific. As a result, there are anomalous low-level easterlies over the equatorial WNP, which generates an anomalous WNP anticyclone that generates negative vorticity. Accordingly, there is an anomalous upper-level WNP cyclone, driving anomalous sinking motion and weakened convection (Figure 12b, d).

The difference between AMJ and JAS is that the IO warming is much weaker during AMJ than during JAS (Figure 12a, c). Consequently, the anomalous low-level easterlies over the equatorial Indo-Pacific and the anomalous WNP low-level anticyclone are weak and insignificant during AMJ but strong and significant during

JAS. This corresponds to weak (strong) IOBM-induced environmental changes during AMJ (JAS) as displayed in Figure 9 (Figure 10).

Figures 14 and 15 display regressions of near-global SSTAs onto the IOBM index during 1979–2022. Both the original and ENSO-independent IOBM indices are normalized for a fair comparison. Warm IOBM events based on the original index during both AMJ and JAS generally relate to eastern Pacific El Niño during the preceding winter (Figure 14a and Figure 15a). For a warm IOBM during AMJ (JAS), El Niño decays relatively faster (slower), while positive SSTAs over the eastern equatorial Pacific persist until the following JAS (OND) (Figure 14c, e, g, i, k and Figure 15c, e, g, i, k). By comparison, there are almost no significant SSTAs regressed onto the ENSO-independent IOBM index over the tropical Pacific (Figure 14b, d, f, h, j, l and Figure 15b, d, f, h, j, l), because the influences of simultaneous and preceding ENSO have been explicitly excluded in this IOBM index.

A warm ENSO-independent AMJ IOBM is characterized by almost no significant SSTAs over other basins during the preceding OND and January–March (JFM) (Figure14b, d), meaning that it is likely to develop locally. During AMJ, when excluding ENSO’s impact, IOBM-induced positive SSTAs substantially weaken and cover a narrower area, while significant SSTAs are concentrated over the western IO (Figure 14f). This means a reduced amplitude of ENSO-independent IO warming, leading to an insignificant IOBM-TC correlation during AMJ. Furthermore, the pattern of the SSTA regressions onto the ENSO-independent IOBM index looks more like a positive phase of the IOD, although the basin-averaged IO SSTA is positive

(Figure 14f). There are also significantly positive SSTAs over the tropical Atlantic (Figure 14f), consistent with a tight connection between western IO warming and tropical Atlantic warming irrespective of ENSO (e.g., Liao and Wang, 2021).

Similarly, a warm ENSO-independent JAS IOBM also tends to develop locally, with warmer SSTAs first occurring over the southwestern IO during the preceding AMJ and then reaching their maxima and covering almost the entire tropical IO during JAS (Figure 15f, h). During JAS, the magnitude and coverage of warm IO SSTAs induced by a warm ENSO-independent IOBM are similar to those induced by a warm original IOBM, meaning that ENSO plays only a minor rule in modulating IOBM-induced SSTAs (Figure 15g, h). This is consistent with a relatively unchanged IOBM-TC relationship after excluding ENSO's influence. Takaya et al. (2018), Ueda et al. (2018) and Zhao et al. (2019) reported a significant warm IO-induced anomalous low-level anticyclonic circulation over the western Pacific during April–September in El Niño-decaying years. These above results imply that the remote influence of IO SSTAs is strengthened by decaying ENSO during AMJ, while it is less affected by ENSO during JAS, owing to the rapid weakening of ENSO from boreal spring to boreal summer.

Although the IO warming does not induce significant environmental changes over the WNP during AMJ and OND, the reasons for these lack of significant modulations differ in different seasons. During OND, the WES feedback weakens substantially, because the SST warming-induced low-level easterlies (Figure 12e) are almost parallel to the climatological winds (Figure 13c). Significant positive SSTAs occur mainly over the Arabian Sea. The associated Kelvin waves have difficulty propagating into the WNP, meaning that the influence of the IOBM is predominately limited to the IO. In addition, there are almost no significant environmental changes at upper levels over the Indo-Pacific region (Figure 12f). This is consistent with the seasonality of the IPOC (Xie et al., 2016), which shows a weakening of the remote influence of IO SSTAs in boreal autumn.

5. Conclusion

This study investigates seasonal changes in the ENSO-independent influence of the IOBM, the dominant mode of IO SST variability, on WNP TC genesis from 1979 to 2022. When excluding the preceding and simultaneous impact of ENSO, we find a significant relationship between annual WNP TC frequency and the annual ENSO-independent IOBM, consistent with previous studies (e.g., Tao et al., 2012). However, the correlation between WNP TC frequency and the ENSO-independent IOBM exhibits obvious seasonality, with a significant correlation during the peak (JAS) season but an insignificant correlation during the early (AMJ) and late (OND) seasons. In a warm IOBM, there are significant WNP TCGF decreases occurring over the region of 15°–25°N and 140°–155°E during JAS. By comparison, there are no significant TCGF changes over almost the entire WNP during AMJ and OND.

The TCGF changes induced by the IOBM during different seasons can be well captured by the corresponding DGPI changes, implying that the seasonality of the IOBM's influence on WNP TC genesis can be explained by related environmental changes. During JAS, the TC-suppressing effect of decreased vorticity and increased sinking motion jointly lead to a reduction of TCGF and DGPI in a warm IOBM, while changes in VWS and MGZW have a minor impact. By contrast, during AMJ and OND, most parts of the WNP show insignificant changes for all environmental variables considered.

Our results highlight the seasonally-dependent mechanism of the IOBM's influence on TC genesis. Compared with previous publications (e.g., Kosaka et al., 2013; Takaya et al., 2018; Ueda et al., 2018; Zhao et al., 2019), we conclude that the IOBM-TC relationship is largely weakened during AMJ when removing the ENSO effect, while it remains significant during JAS and insignificant during OND regardless of whether the ENSO influence is excluded. This feature tends to be jointly caused by the seasonality of the IPOC (Xie et al., 2016) and the seasonal cycle of ENSO. Our results also have important implications for forecasting WNP TC activity during different seasons. Given that there is also seasonality in the modulation of WNP TC genesis by ENSO and the PMM, it is very likely that other climate modes affecting WNP TCs (e.g., tropical North Atlantic SSTAs) should not be considered as a seasonally-consistent forcing. When developing seasonal TC forecasting schemes, we should closely examine how different factors influence TC activity during different seasons.

Data availability statement

All data used in this study are freely available online. Western North Pacific TC best track data recorded by the Joint Typhoon Warning Center, the Japan Meteorological Agency, the China Meteorological Administration and the Hong Kong Observatory are all given in IBTrACS, which is available at: https://www.ncei.noaa.gov/products/international-best-track-archive?name=ib-v4-access. Monthly mean SST data provided by the Hadley Centre Sea Ice and Sea Surface Temperature (HadISST) are obtained from: https://www.metoffice.gov.uk/hadobs/hadisst/data/download.html. The fifth generation European Centre for Medium–Range Weather Forecasts atmospheric reanalysis of the global climate (ERA5) is retrieved from: https://cds.climate.copernicus.eu/cdsapp#!/dataset/reanalysis–era5–pressure–levels–monthly–means?tab=form.

Acknowledgements

This work was jointly funded by the National Natural Science Foundation of China (U2342203, 42192554, 61827901, 42175007, 41905001 and 42305005) and the G. Unger Vetlesen Foundation.

References

Alexander, M. A., I. Bladé, M. Newman, J. R. Lanzante, N. C. Lau, and J. D. Scott, 2002: The atmospheric bridge: The influence of ENSO teleconnections on air-sea interaction over the global oceans. *J. Climate*, **15**, 2205–2231.

An, S. I., 2003: Conditional maximum covariance analysis and its application to the tropical Indian Ocean SST and surface wind stress anomalies. *J. Climate*, **16**, 2932–2938.

Bretherton, C. S., M. Widmann, V. P. Dymnikov, J. M. Wallace, and I. Blade, 1999: The effective number of spatial degrees of freedom of a time-varying field. *J. Climate*, **12**, 1990–2009.

Cai, W., and P. van Rensch, 2013: Austral summer teleconnections of Indo-Pacific variability: Their nonlinearity and impacts on Australian climate. *J. Climate*, **26**, 2796–2810.

Chan, J. C. L., 1985: Tropical cyclone activity in the northwest Pacific in relation to the El Niño/Southern Oscillation phenomenon. *Mon. Wea. Rev.*, **113**, 599–606.

Chan, J. C. L., 2000: Tropical cyclone activity over the western North Pacific associated with El Niño and La Niña events. *J. Climate*, **13**, 2960–2972.

Chen, G., and C. –Y. Tam, 2010: Different impacts of two kinds of Pacific Ocean warming on tropical cyclone frequency over the western North Pacific. *Geophys. Res. Lett.*, **37**, L01803.

Choi, Y., K. Ha, and F. Jin, 2019: Seasonality and El Niño diversity in the relationship between ENSO and western North Pacific tropical cyclone activity.

J. Climate, **32**, 8021–8045.

Du, Y., L. Yang, and S. –P. Xie, 2011: Tropical Indian Ocean influence on Northwest Pacific tropical cyclones in summer following strong El Niño. *J. Climate*, **24**, 315–322.

Du, Y., Z. Chen, S. –P. Xie, L. Zhang, Y. Zhang, and Y. Cai, 2022: Drivers and characteristics of the Indo-western Pacific Ocean capacitor. *Front. Clim.*, **4**, 1014138.

Emanuel, K. A., 1988: The maximum intensity of hurricanes. *J. Atmos. Sci.*, **45**, 1143–1155.

Emanuel, K. A., and D. S. Nolan, 2004: Tropical cyclone activity and global climate. *26th Conf. on Hurricanes and Tropical Meteorology*, Miami, FL, Amer. Meteor. Soc., 240–241.

Emanuel, K., 2018: 100 years of progress in tropical cyclone research. *A Century of Progress in Atmospheric and Related Sciences: Celebrating the American Meteorological Society Centennial, Meteor. Monogr.*, No. 59, 15.1–15.68.

Fu, M., C. Wang, L. Wu, and H. Zhao, 2023: Season-dependent modulation of Pacific Meridional Mode on tropical cyclone genesis over the western North Pacific. *J. Geophys. Res.*, **128**, e2022JD037575.

Gao, S., L. Zhu, W. Zhang, and Z. Chen, 2018: Strong modulation of the Pacific Meridional Mode on the occurrence of intense tropical cyclones over the western North Pacific. *J. Climate*, **31**, 7739–4479.

Gao, S., L. Zhu, W. Zhang, and X. Shen, 2020: Impact of the Pacific Meridional

Mode on landfalling tropical cyclone frequency in China. *Quart. J. R. Meteor. Soc.*, **146**, 2410–2420.

Gill, A. E., 1980: Some simple solutions for heat-induced tropical circulation. *Quart. J. R. Meteor. S.*, **106**, 447–462.

Ha, Y., Z. Zhong, X. Yang, and Y. Sun, 2015: Contribution of East Indian Ocean SSTA to western North Pacific tropical cyclone activity under El Niño/La Niña conditions. *Int. J. Climatol.*, **35**, 506–519.

Hersbach, H., B. Bell, P. Berrisford, S. Hirahara, A. Horányi, J. Muñoz–Sabater, J. Nicolas, C. Peubey, R. Radu, D. Schepers, A. Simmons, C. Soci, S. Abdalla, X. Abellan, G. Balsamo, P. Bechtold, G. Biavati, J. Bidlot, M. Bonavita, G. Chiara, P. Dahlgren, D. Dee, M. Diamantakis, R. Dragani, J. Flemming, R. Forbes, M. Fuentes, A. Geer, L. Haimberger, S. Healy, R. J. Hogan, E. Hólm, M. Janisková, S. Keeley, P. Laloyaux, P. Lopez, C. Lupu, G. Radnoti, P. Rosnay, I. Rozum, F. Vamborg, S. Villaume, and J. Thépaut, 2020: The ERA5 global reanalysis. *Quart. J. R. Meteor. Soc.*, **146**, 1999–2049.

Hong, C., T. Li, LinHo, and Y. Chen, 2010: Asymmetry of the Indian Ocean basinwide SST anomalies: Roles of ENSO and IOD. *J. Climate*, **23**, 3563–3576.

Huangfu, J., W. Chen, T. Ma, and R. Huang, 2018: Influences of sea surface temperature in the tropical Pacific and Indian Oceans on tropical cyclone genesis over the western North Pacific in May. *Clim. Dyn.*, **51**, 1915–1926.

Huangfu, J., W. Chen, R. Huang, and J. Feng, 2019: Modulation of the impacts of the Indian Ocean basin mode on tropical cyclones over the Northwest Pacific during the boreal summer by La Niña Modoki. *J. Climate*, **32**, 3313–3326.

Kim, H. –M., P. J. Webster, and J. A. Curry, 2011: Modulation of North Pacific tropical cyclone activity by three phases of ENSO. *J. Climate*, **24**, 1839–1849.

Klein, S. A., B. J. Soden, and N. C. Lau, 1999: Remote sea surface temperature variations during ENSO: Evidence for a tropical atmospheric bridge. *J. Climate*, **12**, 917–932.

Knapp, K. R., M. C. Kruk, D. H. Levinson, H. J. Diamond, and C. J. Neumann, 2010: The International Best Track Archive for Climate Stewardship (IBTrACS). *Bull. Amer. Meteor. Soc.*, **91**, 363–376.

Kosaka, Y., S. –P. Xie, N. –C. Lau, and G. A. Vecchi, 2013: Origin of seasonal predictability for summer climate over the Northwestern Pacific. *Proc. Natl. Acad. Sci. USA*, **110**, 7574-7579.

Kossin, J. P., K. A. Emanuel, and G. A. Vecchi, 2014: The poleward migration of the location of tropical cyclone maximum intensity. *Nature*, **509**, 349–352.

Lander, M. A., 1994: An exploratory analysis of the relationship between tropical storm formation in the western North Pacific and ENSO. *Mon. Wea. Rev.*, **122**, 636–651.

Lee, T. –C., T. R. Knutson, H. Kamahori, and M. Ying, 2012: Impacts of climate change on tropical cyclones in the western North Pacific basin. Part I: Past observations. *Trop. Cycl. Res. Rev.*, **1**, 213–230.

Li, C., and C. Wang, 2014: Simulated impacts of two types of ENSO events on tropical cyclone activity in the western North Pacific: large–scale atmospheric response. *Climate Dyn.*, **42**, 2727–2743.

Li, R. C. Y., and W. Zhou, 2012: Changes in western Pacific tropical cyclones associated with the El Niño–Southern Oscillation cycle. *J. Climate*, **25**, 5864–5878.

Li, T., B. Wang, C. –P. Chang, and Y. Zhang, 2003: A theory for the Indian Ocean dipole-zonal mode. *J. Atmos. Sci.*, **60**, 2119–2135.

Liao, H., and C. Wang, 2021: Sea surface temperature anomalies in the western Indian Ocean as a trigger for Atlantic Niño events. *Geophys. Res. Lett.*, **48**, e2021GL092489.

Patricola, C. M., S. J. Camargo, P. J. Klotzbach, R. Saravanan, and P. Chang, 2018: The influence of ENSO flavors on western North Pacific tropical cyclone activity. *J. Climate*, **31**, 5395–5416.

Qian, Y., H. Murakami, M. Nakano, P. -C. Hsu, T. L. Delworth, S. B. Kapnick, V. Ramaswamy, T. Mochizuki, Y. Morioka, T. Doi, T. Kataoka, T. Nasuno, and K. Yoshida, 2019: On the mechanisms of the active 2018 tropical cyclone season in the North Pacific. *Geophys. Res. Lett.*, **46**, 12293–12302.

Rayner, N. A., D. E. Parker, E. B. Horton, C. K. Folland, L. V. Alexander, D. P. Rowell, E. C. Kent, and A. Kaplan, 2003: Global analyses of sea surface temperature, sea ice, and night marine air temperature since the late nineteenth century. *J. Geophys. Res.*, **108**, 4407.

Saunders, M. A., R. E. Chandler, C. J. Merchant, and F. P. Roberts, 2000: Atlantic hurricanes and NW Pacific typhoons: ENSO spatial impacts on occurrence and landfall. *Geophys. Res. Lett.*, **27**, 1147–1150.

Song, J., and P. J. Klotzbach, 2018: What has controlled the poleward migration of annual averaged location of tropical cyclone lifetime maximum intensity over the western North Pacific since 1961?. *Geophys. Res. Lett.*, **45**, 1148–1156.

Takaya, Y., Y. Kubo, S. Maeda, and S. Hirahara, 2018: Prediction and attribution of quiescent tropical cyclone activity in the early summer of 2016: case study of lingering effects by preceding strong El Niño events. *Atmos. Sci. Lett.*, **18**, 330–335.

Takaya, Y., 2019: Positive phase of Pacific meridional mode enhanced western North Pacific tropical cyclone activity in summer 2018. *SOLA*, **15A**, 55–59.

Yakaya, Y., I. Ishikawa, C. Kobayashi, H. Endo, and T. Ose, 2020: Enhanced Meiyu-Baiu rainfall in early summer 2020: aftermath of the 2019 super IOD event. *Geophys. Res. Lett.*, **47**, e2020GL090671.

Takaya, Y., Y. Kosaka, M. Watanabe, and S. Maeda, 2021: Skillful predictions of the Asian summer monsoon one year ahead. *Nat. Commun.*, **12**, 2094.

Tao, L., L. Wu, Y. Wang, and J. Yang, 2012: Influences of tropical Indian Ocean warming and ENSO on tropical cyclone activity over the western North Pacific. *J. Meteor. Soc. Japan*, **90**, 127–144.

Timmermann, A., S. I. An, J. S. Kug, F. F. Jin, W. Cai, A. Capotondi, K. M. Cobb, M. Lengaigne, M. J. McPhaden, M. F. Stuecker, K. Stein, A. T. Wittenberg, K. S. Yun, T. Bayr, H. C. Chen, Y. Chikamoto, B. Dewitte, D. Dommenget, P. Grothe, E. Guilyardi, Y. G. Ham, M. Hayashi, S. Ineson, D. Kang, S. Kim, W. Kim, J. Y.

Lee, T. Li, J. J. Luo, S. McGregor, Y. Planton, S. Power, H. Rashid, H. L. Ren, A. Santoso, K. Takahashi, A. Todd, G. Wang, G. Wang, R. Xie, W. H. Yang, S. W. Yeh, J. Yoon, E. Zeller, and X. Zhang, 2018: El Niño–Southern Oscillation complexity. *Nature*, **559**, 535–545.

Ueda, H., K, Miwa, and Y. Kamae, 2017: Seasonal modulation of tropical cyclone occurrence associated with coherent Indo-Pacific variability during decaying phase of El Niño., *J. Meteor. Soc. Japan*, **96**, 381–390.

Walsh, K. J. E., J. L. McBride, P. J. Klotzbach, S. Balachandran, S. J. Camargo, G. Holland, T. R. Knutson, J. P. Kossin, T. –C. Lee, A. Sobel, and M. Sugi, 2016: Tropical cyclones and climate change. *Wiley Interdisciplinary Reviews: Climate Change*, **7**, 65–89.

Wang, B., and J. C. L. Chan, 2002: How strong ENSO events affect tropical storm activity over the western North Pacific. *J. Climate*, **15**, 1643–1658.

Wang, C., C. Li, M. Mu, and W. Duan, 2013: Seasonal modulations of different impacts of two types of ENSO events on tropical cyclone activity in the western North Pacific. *Climate Dyn.*, **40**, 2887–2902.

Wu, Q., J. Zhao, R. Zhan, and J. Gao, 2020: Revisiting the interannual impact of the Pacific Meridional Mode on tropical cyclone genesis frequency in the Western North Pacific. *Climate Dyn.*, **56**, 1003–1015.

Xie, S. –P., and S. G. H. Philander, 1994: A coupled ocean–atmosphere model of relevance to the ITCZ in the eastern Pacific. *Tellus*, **46A**, 340–350.

Xie, S. –P., K. Hu, J. Hafner, H. Tokinaga, Y. Du, G. Huang, and T. Sampe, 2009:

Indian Ocean capacitor effect on Indo–western Pacific climate during the summer following El Niño. *J. Climate*, **22**, 730–747.

Xie, S. –P., Y. Kosaka, Y. Du, K. Hu, J. S. Chowdary, and G. Huang, 2016: Indo-western Pacific ocean capacitor and coherent climate anomalies in post-ENSO summer: a review. *Adv. Atmos. Sci.*, **33**, 411–432.

Yang, J., Q. Liu, S. –P. Xie, Z. Liu, and L. Wu, 2007: Impact of the Indian Ocean SST basin mode on the Asian summer monsoon. *Geophys. Res. Lett.*, **34**, L02708.

Zhan, R., Y. Wang, and X. Lei, 2011a: Contributions of ENSO and East Indian Ocean SSTA to the interannual variability of Northwest Pacific tropical cyclone frequency. *J. Climate*, **24**, 509–521.

Zhan, R., Y. Wang, and C. Wu, 2011b: Impact of SSTA in the East Indian Ocean on the frequency of Northwest Pacific tropical cyclones: a regional atmospheric model study. *J. Climate*, **24**, 6227–6242.

Zhan, R., Y. Wang, and L. Tao, 2014: Intensified impact of East Indian Ocean SST anomaly on tropical cyclone genesis frequency over the western North Pacific. *J. Climate*, **27**, 8724–8739.

Zhang, H., L. Wu, R. Huang, J. –M. Chen, and T. Feng, 2020: Does the Pacific meridional mode dominantly affect tropical cyclogenesis in the western North Pacific?. *Climate Dyn.*, **55**, 3469–3483.

Zhang, W., Y. Leung, and K. Fraedrich, 2015: Different El Niño types and intense typhoons in the western North Pacific. *Climate Dyn.*, **44**, 2965–2977.

Zhang, W., G. A. Vecchi, H. Murakami, G. Villarini, and L. Jia, 2016: The Pacific meridional mode and the occurrence of tropical cyclones in the western North Pacific. *J. Climate*, **29**, 381–398.

Zhao, H., L. Wu, C. Wang, and P. J. Klotzbach, 2019: Consistent late onset of the western North Pacific tropical cyclone season following major El Niño events. *J. Meteor. Soc. Japan*, 97, 673–688.

Zheng, J., Q. Wu, Y. Guo, and S. Zhao, 2016: The impact of summertime North Indian Ocean SST on tropical cyclone genesis over the western North Pacific. *SOLA*, **12**, 242–246.

Zhou, Z. –Q., S. –P. Xie, and R. Zhang, 2021: Historic Yangtze flooding of 2020 tied to extreme Indian Ocean conditions. *Proc. Natl. Acad. Sci. USA*, **118**, e2022255118.

List of Figures

Figure 1. Monthly distributions of lead-lag correlations for (a) monthly ENSO and IOBM indices and for the 3-month mean ENSO index and the IOBM index during (b) AMJ, (c) JAS and (d) OND. Blue, green, orange and red colors refer to the results for the original IOBM index, the IOBM index removing the influence of the simultaneous ENSO, the IOBM index removing the influence of the preceding NDJ ENSO and the IOBM index removing the influences of both the simultaneous ENSO and the preceding NDJ ENSO. Filled dots denote correlations significant at the 0.05 level.

Figure 2. (a) Time series of the annual WNP TC number and the four annual mean IOBM indices investigated in this study from 1979 to 2022. The correlation coefficients between TC number and any IOBM index are given in the legend, while "*" and "**" denote significance at the 0.05 and 0.01 level, respectively. (b) Monthly correlation coefficients between the time series of 3-month running mean WNP TC number and the IOBM indices. Filled dots denote correlations significant at the 0.05 level.

Figure 3. Climatological mean TCGFs over the WNP during (a) AMJ, (b) JAS and (c) OND from 1979–2022.

Figure 4. (a) Regressions of TCGFs onto the (a) original IOBM index during AMJ 1979–2022. (b) As in (a) but for the IOBM index removing the influence of the simultaneous ENSO. (c) As in (a) but for the IOBM index removing the influence of the preceding NDJ ENSO. (d) As in (a) but for the IOBM index removing the influences of both the simultaneous ENSO and the preceding NDJ ENSO,

respectively. Black crosses in (a) –(d) denote regressions significant at the 0.05 level.

Figure 5. As in Figure 4, but for regressions of TCGFs during JAS.

Figure 6. As in Figure 4, but for regressions of TCGFs during OND.

Figure 7. WNP TCGF differences between two phases of the ENSO-independent IOBM for the seasons of (a–c) AMJ, (d–f) JAS and (g–i) OND. The left, middle and right columns refer to the differences of positive IOBM versus neutral, negative IOBM versus neutral and positive IOBM versus negative IOBM, respectively. Identified IOBM seasons are listed in Tables 1–3. Black crosses denote differences significant at the 0.05 level.

Figure 8. (a, c, e) Climatological mean DGPIs and (b, d, f) regressions of DGPIs onto the ENSO-independent IOBM index during (a, b) AMJ, (c, d) JAS and (e, f) OND from 1979–2022. Black crosses denote regressions significant at the 0.05 level.

Figure 9. Regressions of (a) 850–200-hPa VWS, (b) 500-hPa MGZW, (c) 500-hPa vertical velocity and (d) 850-hPa relative vorticity during AMJ onto the ENSO-independent IOBM index from 1979–2022. Black crosses denote regressions significant at the 0.05 level.

Figure 10. As in Figure 9, but for regressions of environmental variables during JAS.

Figure 11. As in Figure 9, but for regressions of environmental variables during OND.

Figure 12. Regressions of environment variables over the Indo-Pacific region onto the IOBM index during (a, b) AMJ, (c, d) JAS and (e, f) OND. Regressed SST and 850-hPa wind vectors are displayed in the left column, while regressed outgoing

longwave radiation and 200-hPa wind vectors are displayed in the right column. Only values of SST and outgoing longwave radiation significant at the 0.05 level are shown. Purple arrows denote regressed wind vectors significant at the 0.05 level.

Figure 13. Climatological mean 850-hPa streamlines over the Indo-Pacific region during (a) AMJ, (b) JAS and (c) OND.

Figure 14. Regressions of near-global SSTAs onto the normalized (a, c, e, g, i, k) original and (b, d, f, h, j, l) ENSO-independent IOBM indices during AMJ in 1979–2022. The subscripts “-1”, “0” and “+1” denote the preceding, current and following years, respectively. Only regressed SSTAs significant at the 0.05 level are shown.

Figure 15. As in Figure 14, but for regressions of near-global SSTAs onto the IOBM indices during JAS.

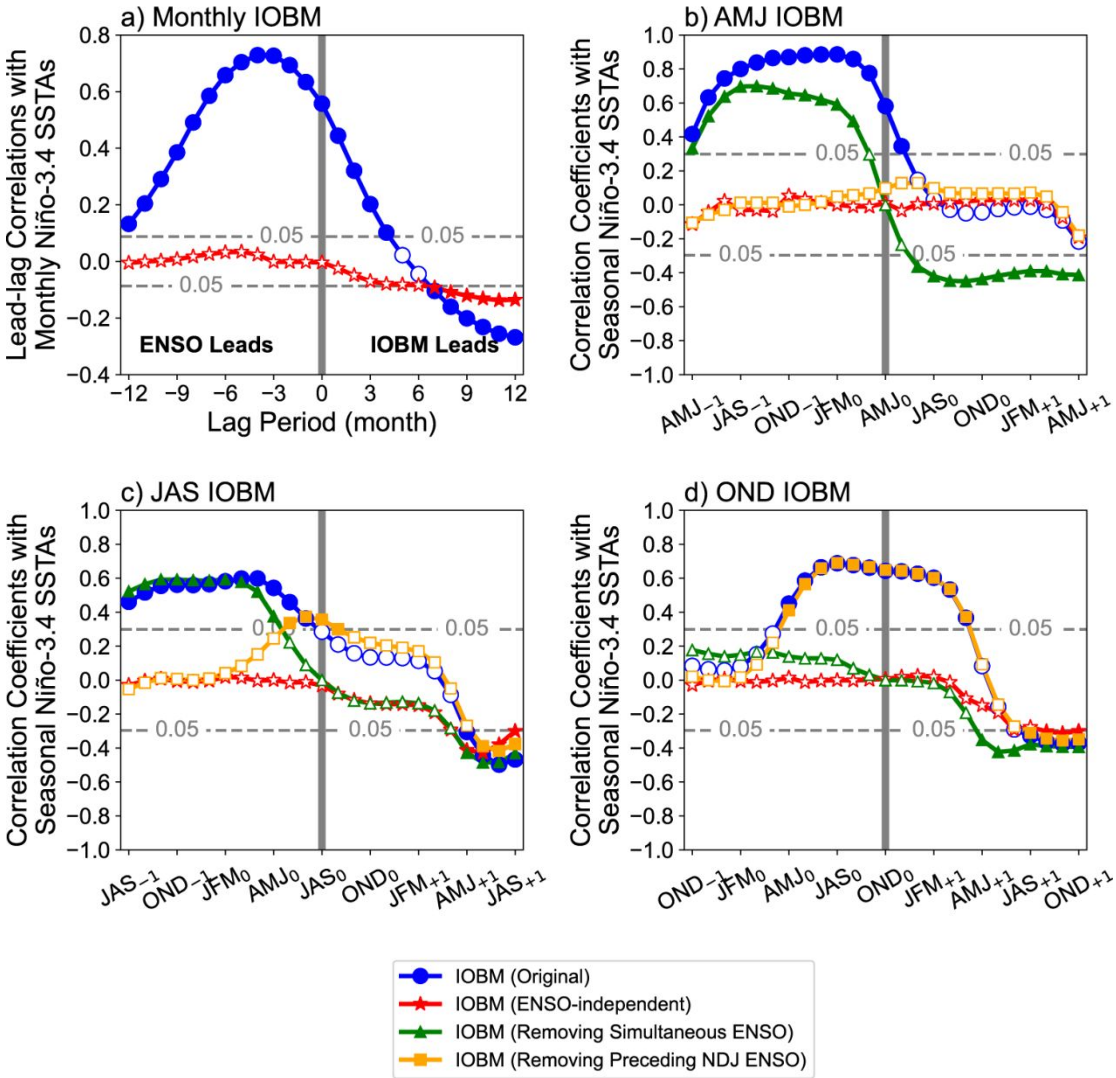

Figure 1. Monthly distributions of lead-lag correlations for (a) monthly ENSO and IOBM indices and for the 3-month mean ENSO index and the IOBM index during (b) AMJ, (c) JAS and (d) OND. Blue, green, orange and red colors refer to the results for the original IOBM index, the IOBM index removing the influence of the simultaneous ENSO, the IOBM index removing the influence of the preceding NDJ ENSO and the IOBM index removing the influences of both the simultaneous ENSO and the preceding NDJ ENSO. Filled dots denote correlations significant at the 0.05 level.

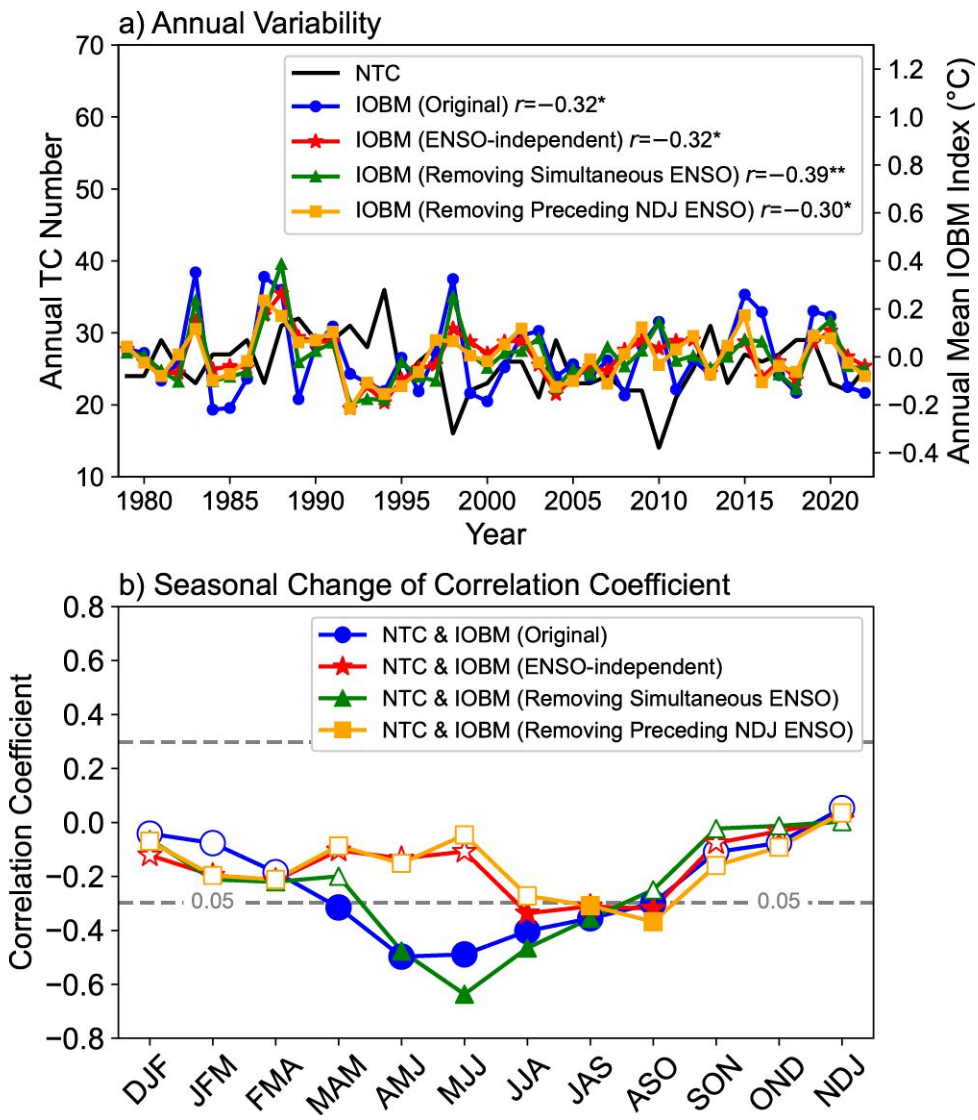

Figure 2. (a) Time series of the annual WNP TC number and the four annual mean IOBM indices investigated in this study from 1979 to 2022. The correlation coefficients between TC number and any IOBM index are given in the legend, while "*" and "**" denote significance at the 0.05 and 0.01 level, respectively. (b) Monthly correlation coefficients between the time series of 3-month running mean WNP TC number and the IOBM indices. Filled dots denote correlations significant at the 0.05 level.

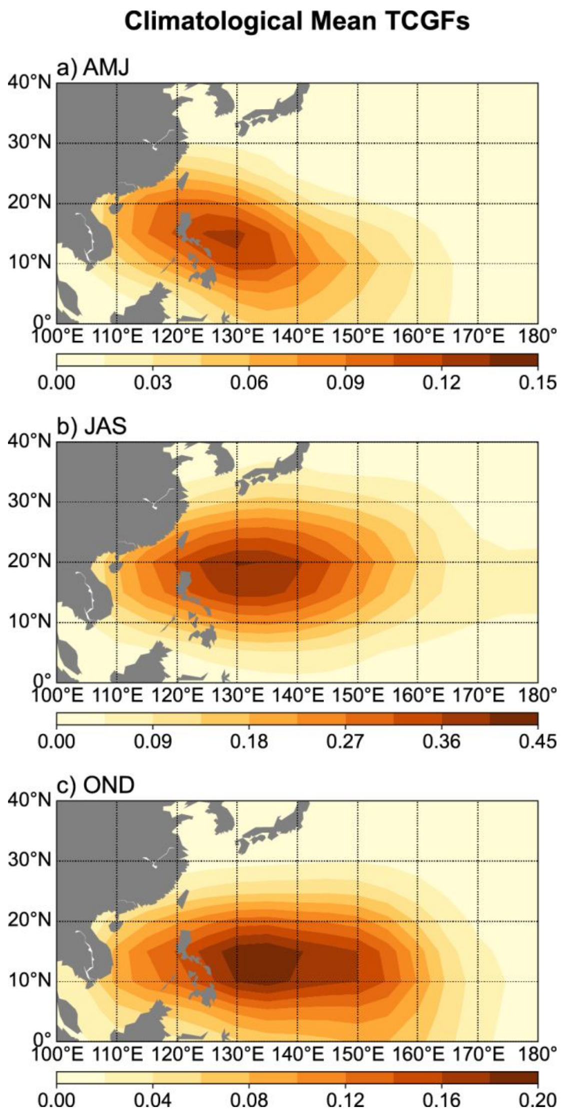

Figure 3. Climatological mean TCGFs over the WNP during (a) AMJ, (b) JAS and (c) OND from 1979–2022.

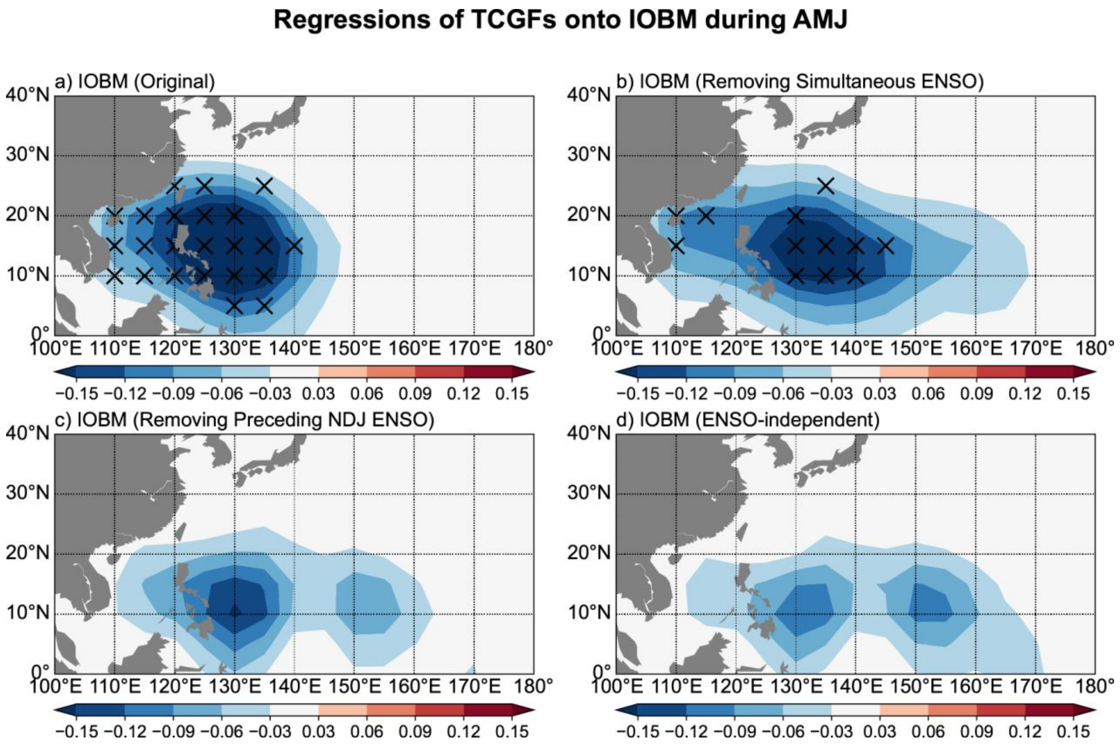

Figure 4. (a) Regressions of TCGFs onto the (a) original IOBM index during AMJ 1979–2022. (b) As in (a) but for the IOBM index removing the influence of the simultaneous ENSO. (c) As in (a) but for the IOBM index removing the influence of the preceding NDJ ENSO. (d) As in (a) but for the IOBM index removing the influences of both the simultaneous ENSO and the preceding NDJ ENSO, respectively. Black crosses in (a) –(d) denote regressions significant at the 0.05 level.

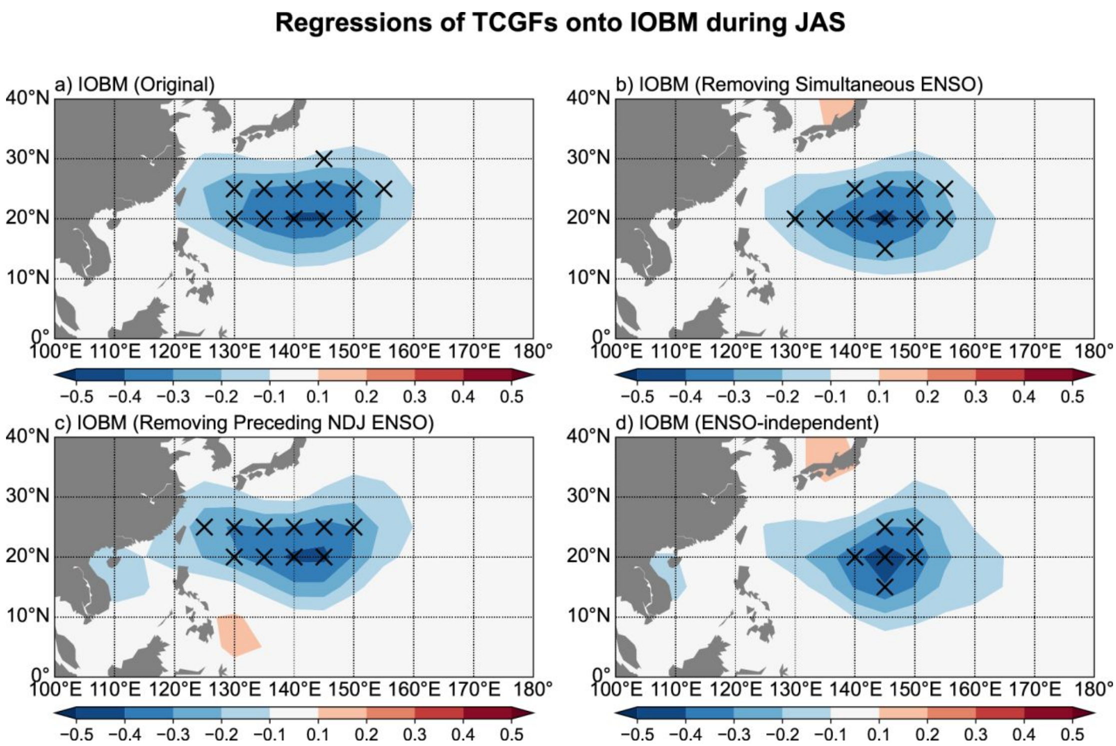

Figure 5. As in Figure 4, but for regressions of TCGFs during JAS.

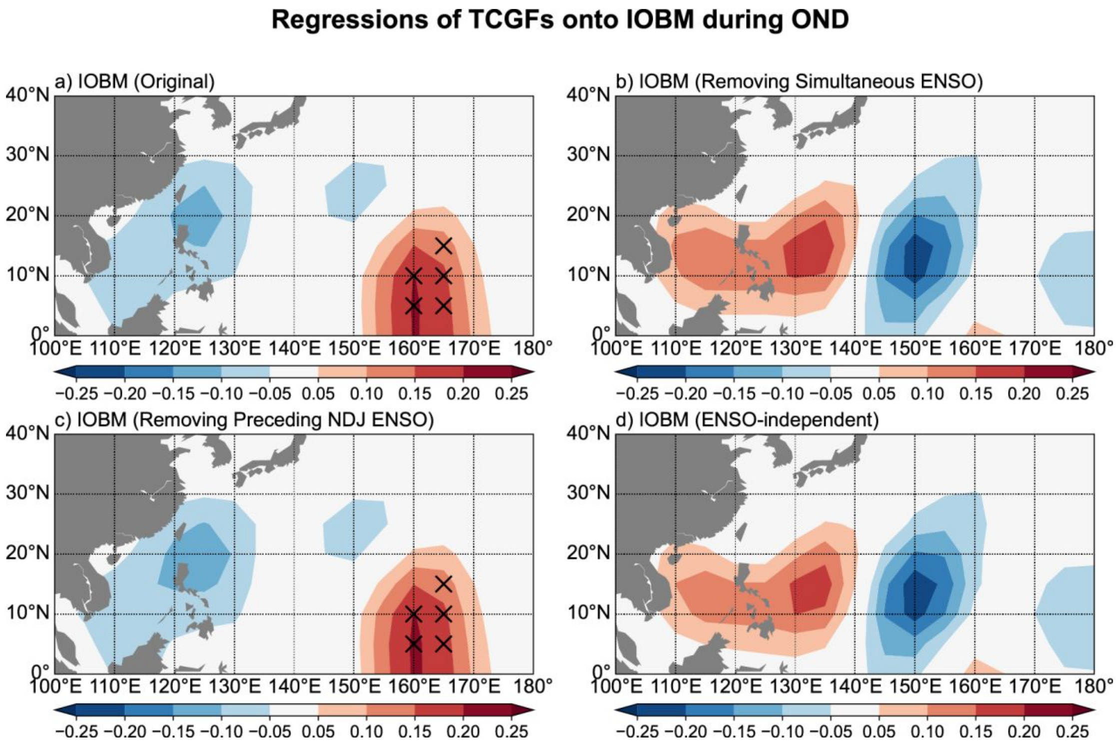

Figure 6. As in Figure 4, but for regressions of TCGFs during OND.

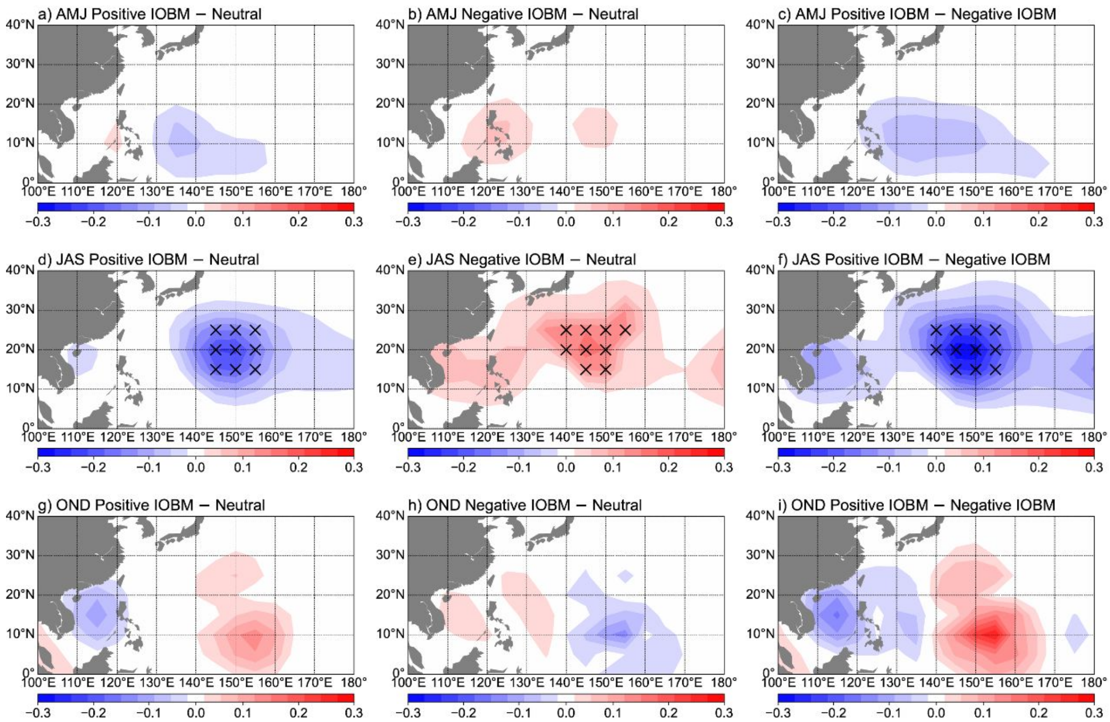

Figure 7. WNP TCGF differences between two phases of the ENSO-independent IOBM for the seasons of (a–c) AMJ, (d–f) JAS and (g–i) OND. The left, middle and right columns refer to the differences of positive IOBM versus neutral, negative IOBM versus neutral and positive IOBM versus negative IOBM, respectively. Identified IOBM seasons are listed in Tables 1–3. Black crosses denote differences significant at the 0.05 level.

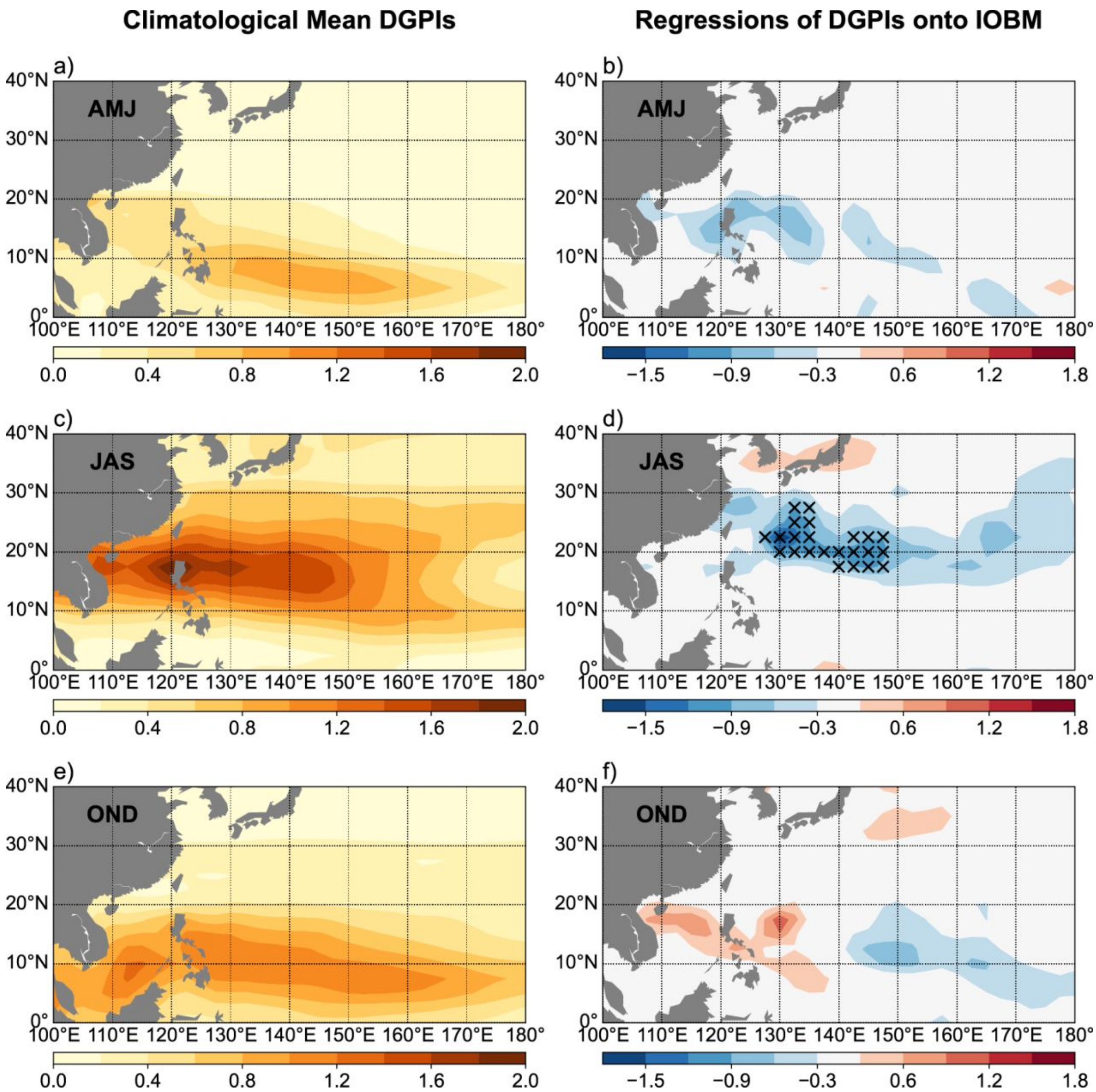

Figure 8. (a, c, e) Climatological mean DGPIs and (b, d, f) regressions of DGPIs onto the ENSO-independent IOBM index during (a, b) AMJ, (c, d) JAS and (e, f) OND from 1979–2022. Black crosses denote regressions significant at the 0.05 level.

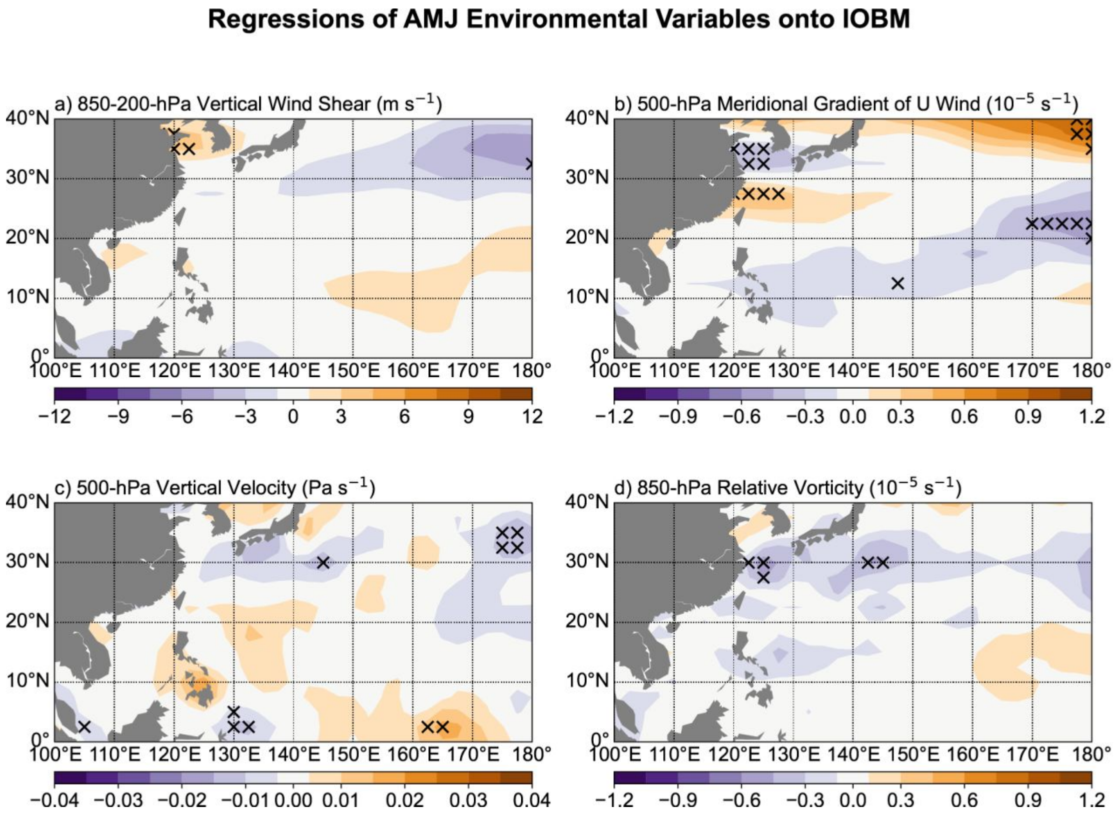

Figure 9. Regressions of (a) 850–200-hPa VWS, (b) 500-hPa MGZW, (c) 500-hPa vertical velocity and (d) 850-hPa relative vorticity during AMJ onto the ENSO-independent IOBM index from 1979–2022. Black crosses denote regressions significant at the 0.05 level.

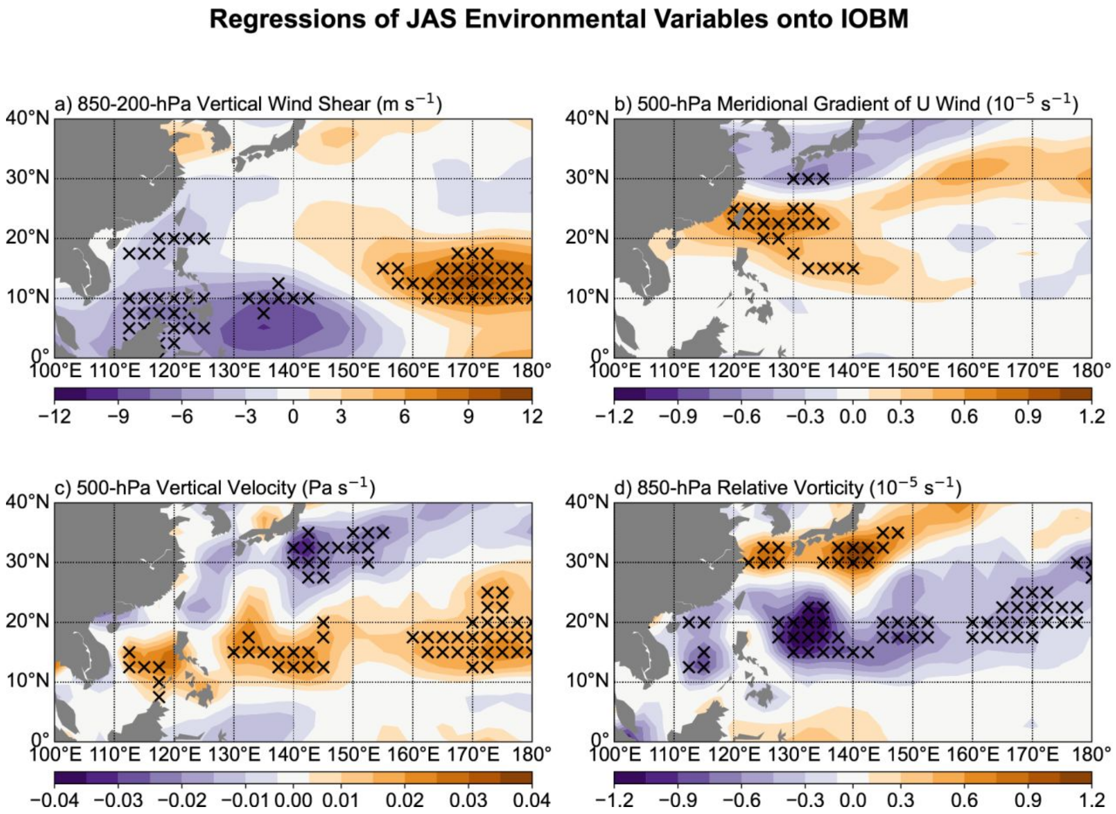

Figure 10. As in Figure 9, but for regressions of environmental variables during JAS.

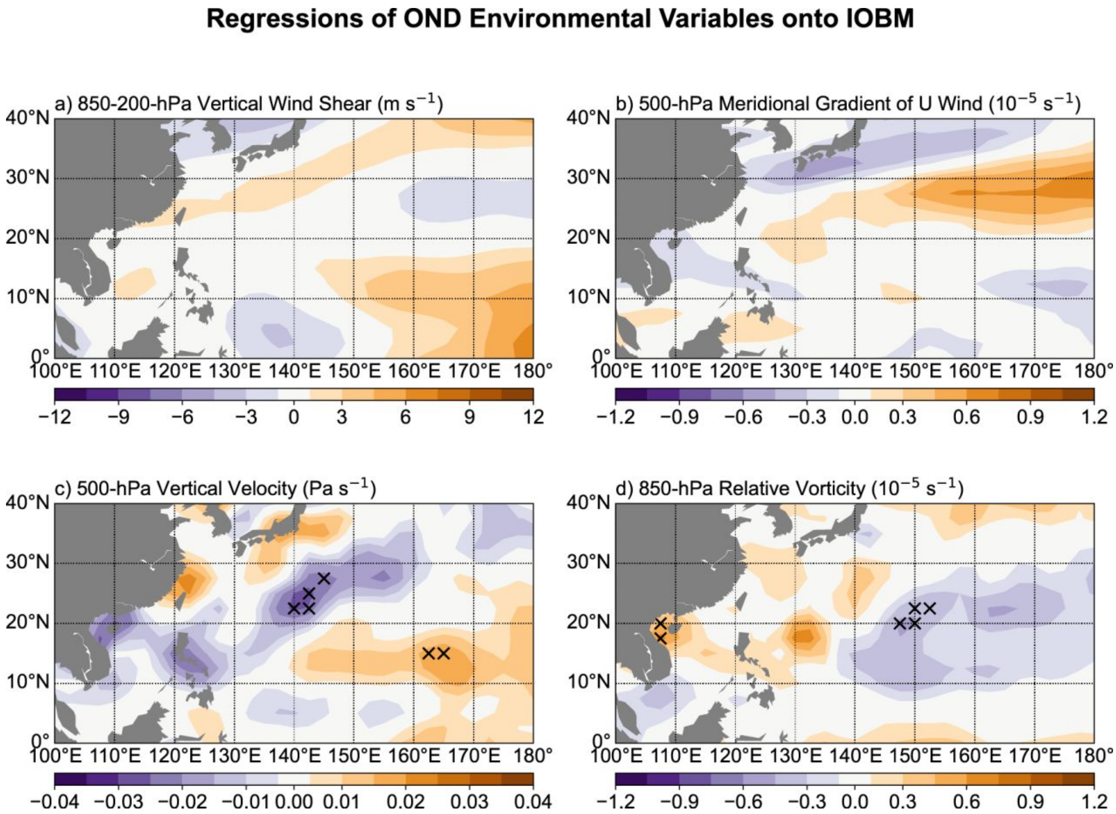

Figure 11. As in Figure 9, but for regressions of environmental variables during OND.

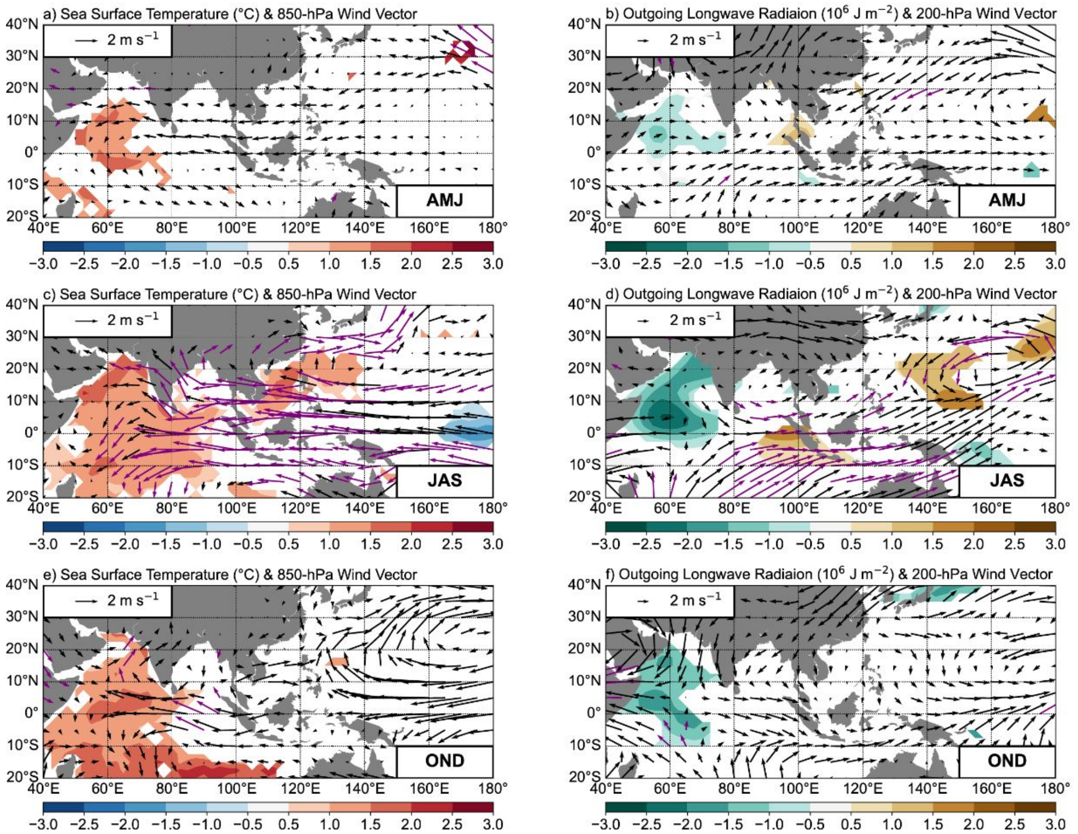

Figure 12. Regressions of environment variables over the Indo-Pacific region onto the IOBM index during (a, b) AMJ, (c, d) JAS and (e, f) OND. Regressed SST and 850-hPa wind vectors are displayed in the left column, while regressed outgoing longwave radiation and 200-hPa wind vectors are displayed in the right column. Only values of SST and outgoing longwave radiation significant at the 0.05 level are shown. Purple arrows denote regressed wind vectors significant at the 0.05 level.

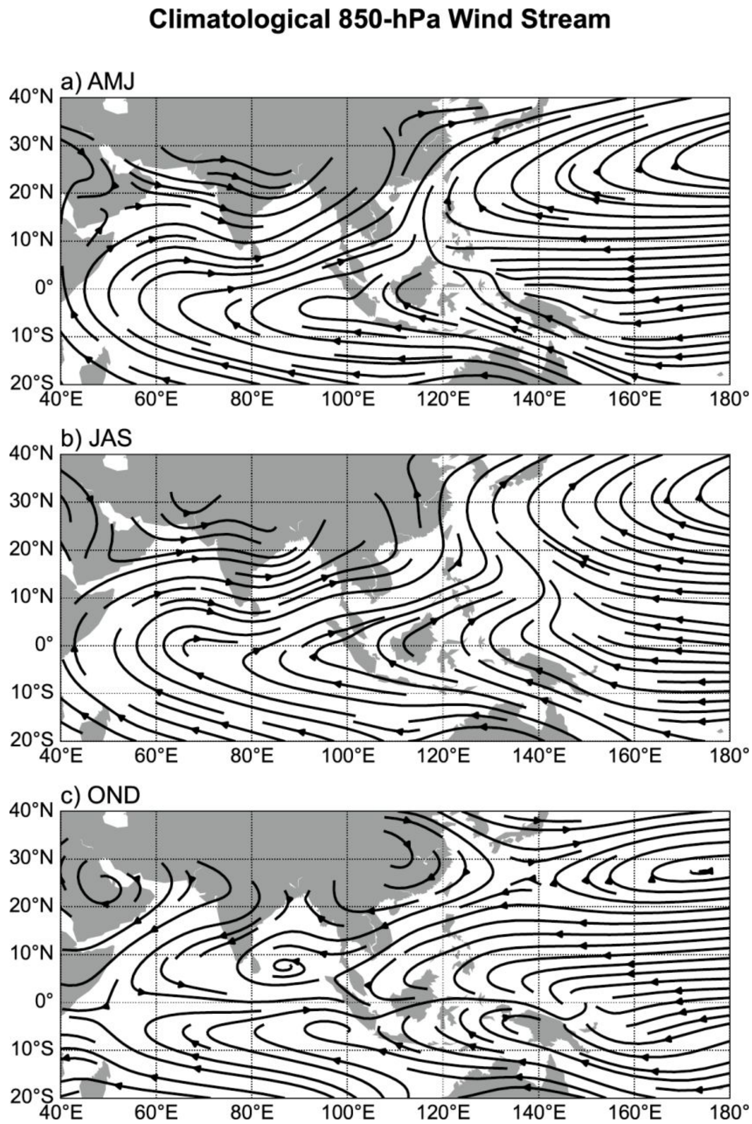

Figure 13. Climatological mean 850-hPa streamlines over the Indo-Pacific region during (a) AMJ, (b) JAS and (c) OND.

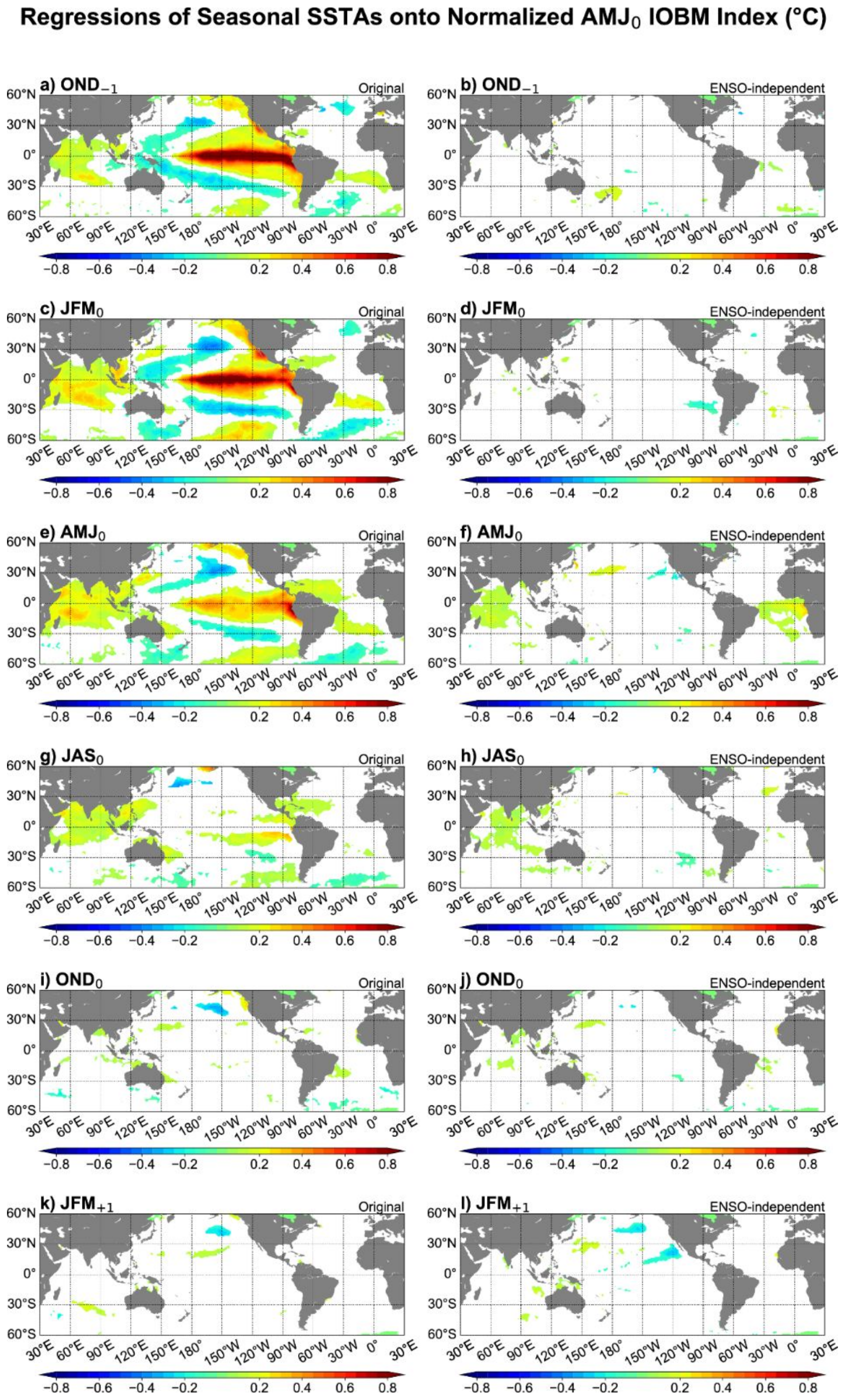

Figure 14. Regressions of near-global SSTAs onto the normalized (a, c, e, g, i, k) original and (b, d, f, h, j, l) ENSO-independent IOBM indices during AMJ in 1979–2022. The subscripts "-1", "0" and "+1" denote the preceding, current and following years, respectively. Only regressed SSTAs significant at the 0.05 level are shown.

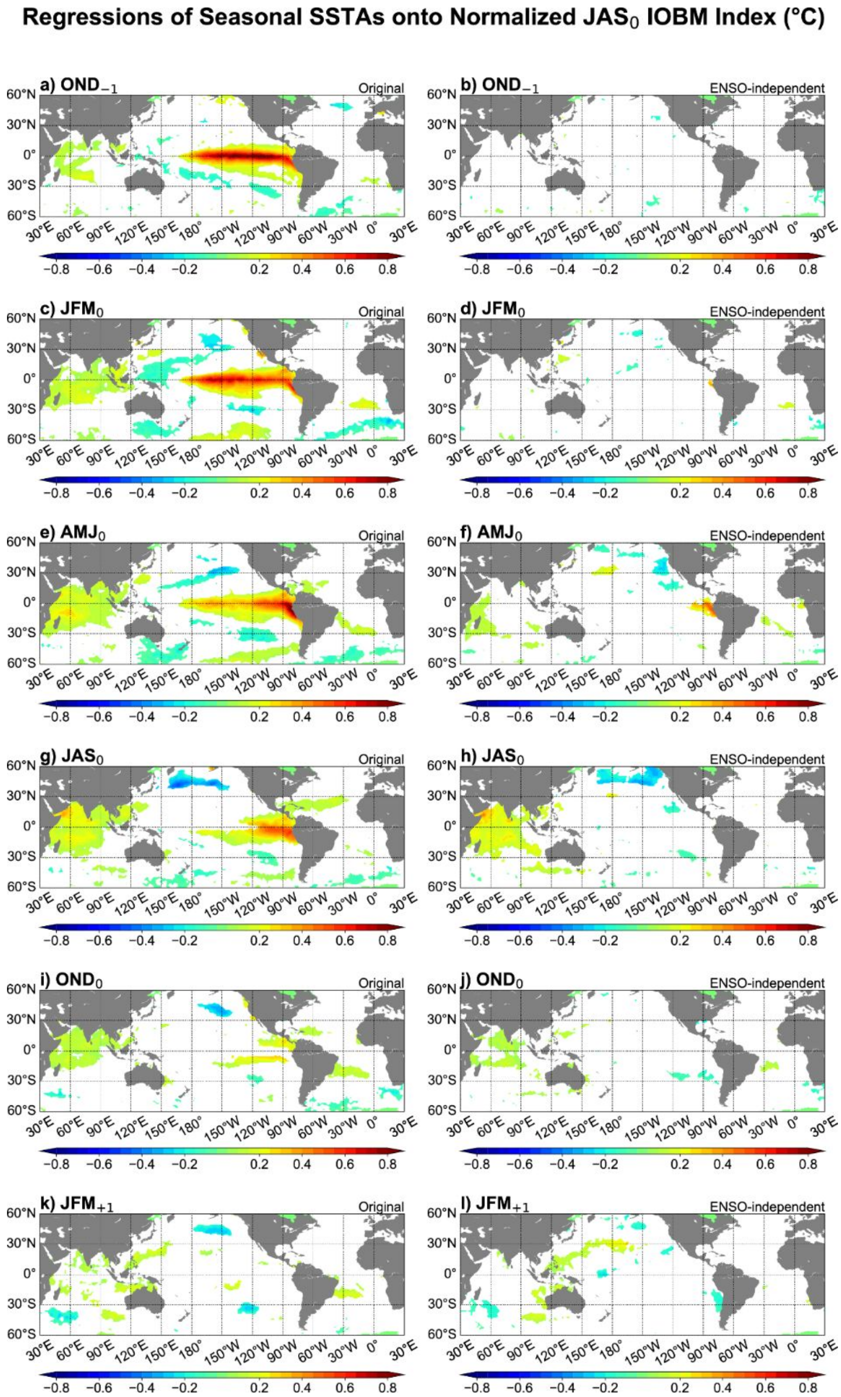

Figure 15. As in Figure 14, but for regressions of near-global SSTAs onto the IOBM indices during JAS.

List of Tables

Table 1. List of AMJ seasons with positive, neutral and negative IOBM phases, as well as corresponding TC frequencies over the WNP.

Positive IOBM		Neutral		Negative IOBM	
Year	TC Frequency	Year	TC Frequency	Year	TC Frequency
1991	3	1979	3	1995	2
1998	0	1980	6	2004	8
2001	3	1981	5	2013	4
2009	4	1986	5		
2014	4	1990	5		
2020	2	1994	4		
		1996	3		
		2002	4		
		2003	5		
		2005	2		
		2006	3		
		2007	2		
		2010	0		
		2012	5		
		2017	2		
		2018	4		
		2021	4		
Mean	2.7	Mean	3.6	Mean	4.7

Table 2. As in Table 1, but for JAS.

Positive IOBM		Neutral		Negative IOBM	
Year	TC Frequency	Year	TC Frequency	Year	TC Frequency
1983	10	1979	12	1992	17
2003	10	1980	12	1993	17
2008	10	1981	16	1994	24
2020	11	1984	14	1996	17
		1986	11	2013	17
		1990	14	2016	18
		1991	15		
		1995	13		
		2000	16		
		2001	16		
		2005	15		
		2006	12		
		2014	11		
		2017	17		
		2018	18		
		2019	15		
		2021	11		
Mean	10.3	Mean	14.0	Mean	18.3

Table 3. As in Table 1, but for OND.

Positive IOBM		Neutral		Negative IOBM	
Year	TC Frequency	Year	TC Frequency	Year	TC Frequency
1980	6	1979	7	1981	7
1989	8	1990	9	1992	10
2001	7	2003	5	1993	9
2013	8	2008	6	1996	5
		2012	7	2005	4
Mean	7.3	Mean	6.8	Mean	7.0

Table 4. Correlation coefficients between TC frequency and environmental factors during different seasons and over different regions from 1979 to 2022. "*", "**" and "***" denote significance at the 0.05, 0.01 and 0.001 level, respectively.

	TC Frequency			
	AMJ 5°–25°N 110°–170°E	JAS 10°–30°N 120°–170°E	OND 5°–25°N 105°–140°E	OND 5°–30°N 140°–160°E
DGPI	0.85***	0.52***	0.65***	0.42**
850–200-hPa VWS	-0.39**	-0.01	-0.23	-0.06
500-hPa MGZW	-0.50**	-0.34*	-0.39**	-0.24
500-hPa Vertical Velocity	-0.71***	-0.46**	-0.60***	-0.34*
850-hPa Relative Vorticity	0.78***	0.39**	0.55***	0.58***